An explanation of the highly efficient magnetic quenching of fluorescence in intermediate case molecules based on two manifold models

doi: 10.1063/1.469655

An explanation of the highly efficient magnetic quenching of fluorescence in intermediate case molecules based on two manifold models

Hirohiko Kono
Chemistry, Division of Science, Graduate School, Tohoku University, Kawauchi North Campus, Kawauchi, Sendai 980-77, Japan

Nobuhiro Ohta
Graduate School of Engineering, Division of Molecular Chemistry, Faculty of Engineering, Hokkaido University, Sapporo 060, Japan

(Received 24 February 1995; accepted 27 March 1995)

The magnetic quenching of fluorescence in intermediate case molecules is modeled by including two triplet manifolds $\{|b_j\rangle\}$ and $\{|c_j\rangle\}$ mutually shifted by the zero-field splitting $E_{\rm gap}$ (though a triplet has three spin sublevels); the $\{|b_j\rangle\}$ are coupled to a bright singlet state $|s\rangle$ by intramolecular interaction V and the two manifolds are coupled by a magnetic field. For the two manifold Bixon–Jortner model where the level spacings and the couplings to $|s\rangle$ are constant and no spin–vibration interactions exist (the Zeeman interaction connects only the spin sublevels of the same rovibronic level j), there are two sets of field dressed eigenstates, $\{|\hat{b}_j\rangle\}$ and $\{|\hat{c}_j\rangle\}$, of the background Hamiltonian $\mathbf{H}-V$. $|\hat{b}_j\rangle$ and $|\hat{c}_j\rangle$ are liner combinations of $|b_j\rangle$ and $|c_j\rangle$. We call the energy structure ''eclipsed (E)'' when the two sets of dressed states overlap in energy and call it ''staggered (S)'' when every $|\hat{b}\rangle$ state is just between two adjacent $|\hat{c}\rangle$ states. The E and S structures alternatively appear with increasing Zeeman energy h_Z. As h_Z increases, the number of effectively coupled background levels, $N_{\rm eff}$, increases for the S structure but remains unchanged for the E structure. The S structure is in accord with the experimental result that the quantum yield is reduced to 1/3 at anomalously low fields ($h_z/E_{\rm gap}\ll 1$): in the far wing regions of the absorption band the mixing between the manifolds is determined by the ratio $h_Z/E_{\rm gap}$, but near the band center the intermanifold mixing is enhanced by the presence of $|s\rangle$. Using a random matrix approach where $\mathbf{H}$ is constructed of the rotation–vibration Hamiltonians H_B and H_C arising from the manifolds $\{|b_j\rangle\}$ and $\{|c_j\rangle\}$, we show that an S structure can be formed in real molecules by nonzero $\Delta H_{BC}\equiv H_B-H_C-E_{\rm gap}$ ($E_{\rm gap}$ is the zero-field splitting at the equilibrium nuclear configuration). Indirect spin–vibration interactions lead to $\Delta H_{BC}\neq 0$; the vibrational ΔH_{BC} caused by spin–spin and vibronic interactions and the rotational ΔH_{BC} caused by spin–rotation and rotation–vibration interactions. The matrix elements of $\mathbf{H}$ are written down in terms of the eigenfunctions $\{|j\rangle\}$ of the average Hamiltonian $(H_B+H_C)/2$. If the vibrational modes are strongly coupled (the energies of levels are given by a Wigner distribution and the coupling strengths are given by a Gaussian distribution), the vibrational $\langle j|\Delta H_{BC}|j'\rangle$ for wave functions of roughly the same energy are Gaussian random. As the rms of $\langle j|\Delta H_{BC}|j'\rangle$ approaches the average level spacing (on excitation into higher vibrational levels), the efficiency of magnetic quenching becomes as high as in the S case. Nonzero $\langle j|\Delta H_{BC}|j'\rangle$ let isoenergetic levels belonging to different manifolds vibrationally overlap: the ΔH_{BC}, together with the magnetic field, causes level repulsion leading to the S structure and opens up isoenergetic paths between the manifolds. The efficient magnetic quenching in pyrazine can be explained by the vibrational ΔH_{BC}, since the S_1-T_1 separation is as large as 4500 $\rm cm^{-1}$. If Coriolis couplings cause K scrambling considerably, the rotational ΔH_{BC} mixes $\{|j\rangle\}$. This mechanism explains the rotational dependence of magnetic quenching in s-triazine of which S_1-T_1 separation is only $\sim$1000 $\rm cm^{-1}$. © *1995 American Institute of Physics.*

I. INTRODUCTION

Radiationless transition is a change in the electronic state of a molecule.[1–6] In many cases, two electronic states (or two potential surfaces) are involved in a radiationless process. The conventional model to describe the process is as follows:[1–7] a ''bright'' level $|s\rangle$ (carrying optical transition probability) is coupled to a more dense manifold of background vibronic (rovibronic) levels $\{|b_j\rangle\}$ by an intramolecular interaction V. For intersystem crossing (ISC), $|s\rangle$ is a vibronic level of a singlet (e.g., S_1) and $\{|b_j\rangle\}$ is a set of vibronic levels in a triplet; the subscript j denotes the rotation–vibration levels in the triplet. V is the spin–orbit coupling. In the case where the direct spin–orbit coupling between the singlet and triplet vanishes, there is a chance for second-order processes to couple the two electronic states. In that case, V is written as a product combination of two interaction operators (e.g., the spin–orbit operator and the vibronic interaction operator).[8]

The selection rules for radiationless transitions in intermediate case molecules such as pyrazine can be adequately described in Hund's coupling case (b).[9–12] Among the quantum numbers used are the rotational angular momentum N, electron spin angular momentum S, and total angular momentum J. Interactions involving nuclear spins are ignored

 0021-9606/95/103(1)/162/20/$6.00

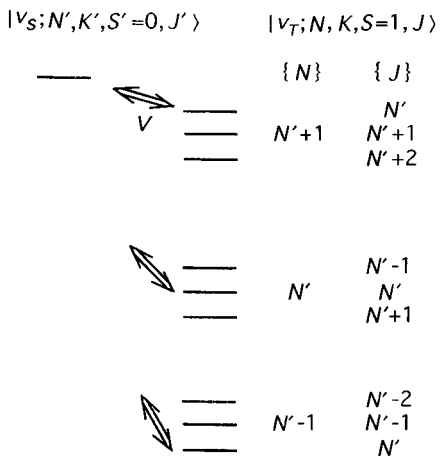

FIG. 1. A schematic illustration of spin splitting. The $|v_S;N',S'=0,J'=N'\rangle$ and $|v_T;N,S=1,J\rangle$ denote singlet and triplet levels, respectively (v_S and v_T denote rovibronic states of the singlet and triplet). Each $|v_T;N,S=1,J\rangle$ level is split into three spin sublevels. The spin sublevels belonging to a rovibronic level $|v_T;N\rangle$ have different $J=N+1,N,N-1$. In the absence of external field, only one of them that satisfies the selection rule $\Delta J=0$ is coupled to $|v_S;N',S',J'\rangle$.

in this paper. The singlet and triplet levels are then denoted by $|v_S;N',S'=0,J'=N'\rangle$ and $|v_T;N,S=1,J\rangle$, respectively (where v_S and v_T denote rovibronic states of the singlet and triplet). Each $|v_T;N,S=1,J\rangle$ level is split into three spin sublevels by spin–spin and spin–orbit interactions. A schematic illustration of spin splitting is drawn in Fig. 1. The spin sublevels belonging to a rovibronic level $|v_T;N\rangle$ have different $J=N+1,N,N-1$. These sublevels are denoted by the fine structure components F_1, F_2, and F_3, respectively.

We restrict ourselves to gas phases at low pressures. In the absence of external field, the space is isotropic: the total angular momentum J is conserved in ISC, i.e., $J=J'$.[10–12] The selectively excited singlet level $|v_S;N'S'J'\rangle$ is coupled by V to three levels of a $|v_T\rangle$ manifold, those with $J=J'=N'$ of the spin sublevels. The arrows ($\Leftrightarrow$) in Fig. 1 represent such couplings. Of the three spin sublevels belonging to the same rovibronic level $|v_T;N\rangle$, i.e., of F_1, F_2, and F_3, only one level is coupled to $|v_S;N'S'J'\rangle$.

If an external magnetic field is applied, the $\Delta J=0$ selection rule is no longer meaningful. When the magnetic field is strong enough to fully decouple the electron spin S from the molecular axis, the spin sublevels with different J are mingled among one another by the Zeeman interaction, and the singlet level can interact with all the triplet spin sublevels.[10–16] At zero field, the three sublevels F_1, F_2, and F_3 are split from one another by the order of GHz (in Hund's case (b) the zero-field splittings of spin sublevels are assumed to be much smaller than the separation between adjacent rotational levels). As the Zeeman energy becomes larger than the zero-field splittings, the magnetic field mingles the spin sublevels sufficiently: the number of the rovibronic levels effectively coupled to $|s\rangle$, N_{eff}, is expected to increase by a factor of 3 and the probability of returning to $|s\rangle$ will be reduced to 1/3 of that at zero field. For pyrazine, the zero-field splittings are on the order of 1 GHz,[17] which means that 300 G in magnetic field strength is expected to be necessary for a substantial sublevel mixing or for a substantial reduction in the quantum yield (30 GHz is equivalent to 10^4 G for $g=2$). What have been measured are however controversial; appreciable quenching occurs at fields that are as small as 20 G.[18–24]

Matsumoto *et al.*[18,19] have suggested, as one reasonable explanation, that the ''Zeeman mixing process'' connects the sublevel components of different rovibronic levels. The process is called ''intervibronic mixing.'' This idea seems to be supported by experimental observations that the efficiency of magnetic quenching increases with increasing vibrational level density in the triplet state (for pyrazine, the average spacing between adjacent vibronic levels near the S_1 origin is less than 0.3 GHz if all the rovibronic levels are counted).[25] The vibrational state dependence of the fluorescence quantum yield and the time resolved decay lead to an important fact that magnetic quenching is more efficient on excitation into higher vibrational level in S_1 than on excitation into the vibrationless level.[20–24,26] It has also been reported that magnetic quenching becomes more efficient with increasing J'.[18–24] The observation suggests that N_{eff} increases with increasing J'. Presumably, Coriolis coupling in the triplet breaks down the $\Delta K=0$ selection rule (K is the projection of N onto the molecular fixed axis). This is called ''K scrambling.''[6,27–30]

However, unless spin and vibration are directly or indirectly coupled to each other, the Zeeman interaction cannot directly connect the spin sublevels of different rovibronic levels. What it directly connects are the different sublevels of the same rovibronic level (intravibronic mixing). Without spin–vibration interaction, the overlaps between the spin sublevels of different rovibronic levels vanish. Coriolis coupling alone does not induce intervibronic mixing. This can be clarified by using a representation in which Coriolis coupling is diagonalized. We believe that some kind of ''mechanism'' is hidden behind the idea of intervibronic mixing. The purpose of this paper is to find out the mechanism of intervibronic mixing and to explain why the quantum yield is reduced to 1/3 at anomalously low fields.

In this paper, the effect of magnetic field on ISC is modeled by adding another background manifold $\{|c_j\rangle\}$ coupled to $\{|b_j\rangle\}$; the coupling between the sublevels $|b_j\rangle$ and $|c_j\rangle$ is induced by a magnetic field (in the absence of spin–vibration interaction the Zeeman interaction mingles only the spin sublevels of the same rovibronic level j). A manifold means a set of rovibronic levels that have the same total angular momentum J. The term ''intervibronic'' can be put into ''intermanifold excluding intravibronic.'' The background manifold $\{|b_j\rangle\}$ is a set of rovibronic levels that are directly coupled to $|s\rangle$ by the intramolecular interaction V, e.g., $\{|v_T;N=N',S=1,J=N'\rangle\}$, and the manifold $\{|c_j\rangle\}$ is a set of rovibronic levels that are not directly coupled to $|s\rangle$, e.g., $\{|v_T;N=N',S=1,J=N'+1\rangle\}$. A manifold can be associated with a potential surface that yields the vibronic levels $\{|v_T\rangle\}$. Without spin–vibration interaction, the potential surfaces corresponding to different manifolds are of the same form and mutually shifted in energy by the zero-field splittings.

We deal with the two manifold model, though a triplet

electronic state has three spin sublevels. Our model will serve as a prototype to draw characteristic features of the magnetic field effect on ISC. The model is treated in Secs. III and IV on the basis of the assumptions used in the Bixon–Jortner model[7] (equally spaced background levels with a constant coupling to $|s\rangle$). A random matrix approach is also used in Sec. V to take into account level statistics.[31] We examine how the nearest-neighbor spacing distribution and the coupling strength fluctuation affect the magnetic quenching. The role of indirect spin–vibration interactions in magnetic quenching is also examined in Sec. V.

II. PRELIMINARIES

In this introductory section, we outline the eigenstate approach to time-resolved studies of an excited molecule and review the relation between the time-resolved fluorescence pattern and the level statistics. To relate our model with experimental observables, we make connections among the magnetic field strength, quantum yield, and N_{eff}.

A. Time evolution and level statistics

The time evolution of a molecule undergoing radiationless transitions can be described as follows. As usual, we suppose that a ''bright'' level $|s\rangle$ is coupled to a more dense manifold of background rovibronic levels $\{|b_j\rangle\}$ through an intramolecular interaction V. The eigenfunctions $|n\rangle$ of the molecular Hamiltonian H can be expressed as a liner combination of the zero-order levels

$$|n\rangle = a_n|s\rangle + \sum_j b_{nj}|b_j\rangle, \tag{1}$$

$$H|n\rangle = \hbar\omega_n|n\rangle, \tag{2}$$

where the coefficients are determined by the energies of $|s\rangle$ and $\{|b_j\rangle\}$ and by the couplings v_{sj} between $|s\rangle$ and $\{|b_j\rangle\}$. The s-level character is distributed among eigenfunctions. We denote the full width at half-maximum (FWHM) of distribution by ΔE.

The time evolution of the system can be described in terms of $\{|n\rangle\}$. The initially prepared state is identical to the nonstationary $|s\rangle$ level when the pulse duration is shorter than $\hbar/\Delta E$.[7,32,33] For such excitation, the time dependence of the initially prepared state is written as

$$|\Psi(t)\rangle = \exp(-iHt/\hbar)|s\rangle = \sum_n a_n^*|n\rangle e^{-i\omega_n t}. \tag{3}$$

The time evolution of the fluorescence intensity, $I_f(t)$, can be determined by projecting out of this wave function the bright level character $|s\rangle$:

$$\begin{aligned} I_f(t) &= \Gamma_s|\langle s|\Psi(t)\rangle|^2 \\ &= \Gamma_s\left\{\sum_n |a_n|^4 e^{-\gamma_n t} + 2\sum_{n<m}\sum |a_n|^2|a_m|^2 \right. \\ &\quad \left. \times\cos[(\omega_n-\omega_m)t]e^{-(\gamma_n+\gamma_m)t}\right\}, \end{aligned} \tag{4}$$

where we have included the radiative rate of $|s\rangle$, Γ_s, and the longitudinal relaxation rate of the eigenstate $|n\rangle$, γ_n. Throughout this paper, the ''intermediate case'' is assumed, that is, the average level spacing ε and the average coupling v are assumed to fulfill the relations $\varepsilon > \hbar\gamma_n$ and $v \geqslant \varepsilon$.

The first sum represents the population decays of individual eigenstates (incoherent contribution) and the second one represents the s-character interference among eigenstates (coherent contribution).[29,30,34,35] The coherent excitation over the bandwidth ΔE results in a rapid phase collapse (''dephasing'') among the eigenstates excited. The dephasing at early times ($t < \hbar/\Delta E$) is purely exponential if the s-character distribution function (absorption profile) is a Lorentzian, that is, for the case of equally spaced, equally coupled $|b_j\rangle$ levels (the so-called Bixon–Jortner model).[7] Even for randomly spaced, randomly coupled $|b_j\rangle$ levels it is very close to exponential.[35] The decay constant for this fast dephasing, γ_C, is generally equal to ΔE. The FWHM ΔE is approximately given as

$$\gamma_C = \Delta E = \frac{2\pi v^2}{\varepsilon}. \tag{5}$$

Strong recurrences of fluorescence occur at integer multiples of time $t = 2\pi\hbar/\varepsilon$ if the eigenstates $\{|n\rangle\}$ are equally spaced by ε (for equally spaced, equally coupled $|b_j\rangle$ levels the resultant eigenstate are nearly equally spaced). This type of recurrence is ascribed to the coherent term. For a random distribution of energy levels, such recurrences are smeared out and only slight undulations are observed; they become negligible once the coherent contribution fully decays, i.e., after $t > \hbar/\Delta E$ (especially when ensemble averages, such as over the rotational constant K, are necessary). The slow decay after $t > \hbar/\Delta E$ thus comes mainly from the sum of incoherent decays of individual eigenstates.[34,35]

The energy levels for a set of independent oscillators (integrable system) are independently distributed in the energy axis. A collection of those levels will have many levels close or overlapping. The distribution $P(S)$ of nearest-neighbor spacings S exhibits ''level clustering'' ($P \neq 0$ at $S = 0$), and fits the Poisson distribution[29–31] (except for the case where the system is harmonic)[36]

$$P(S) = \frac{1}{D}\exp\left(-\frac{S}{D}\right), \tag{6}$$

where D is the local average spacing. If the level spacing distribution is given by a Poisson distribution, the fluorescence decay is characterized by the biexponential form

$$I_f(t) = \Gamma_s[A_I\exp(-\gamma_I t) + A_C\exp(-\gamma_C t)]. \tag{7}$$

The decay constant for the incoherent component, γ_I, is considered the average of $\{\gamma_n\}$ over the eigenstates in ΔE.

For a set of strongly coupled oscillators, the mode couplings will split some of degeneracies, shifting the distribution towards larger spacings. In the extreme limit represented by completely random matrices, such as the Gaussian orthogonal ensemble (GOE), the distribution is accurately characterized by the Wigner surmise which exhibits ''level repulsion'' ($P = 0$ at $S = 0$)[31]

$$P(S)=\frac{\pi}{2}\frac{S}{D^2}\exp\left[-\frac{\pi}{4}\left(\frac{S}{D}\right)^2\right]. \tag{8}$$

The distribution has its peak at $S\approx 0.8D$. This level correlation causes a depression of the fluorescence intensity just after the decay of the fast component.[35] This depression is called the correlation hole, which Huber *et al.*[37] have detected in fluorescence decays following excitation of jet-cooled butynal. In this case, $\exp(-\gamma_I t)$ in Eq. (7) should be replaced with[38,39]

$$[1-b_2(Dt)]\exp(-\gamma_I t),$$

where $b_2(t)$ is the Fourier transform of the two-level cluster function $Y_2(\omega)$[31] [the function $1-Y_2(\omega)$ gives the probability of observing a level at a distance ω from a given level].

Some other distribution functions have been proposed to cover intermediate regimes between the two extreme limits (namely, the Poisson and Wigner distributions). Among them is the Brody distribution with the "repulsion parameter" r.[31,40] Given a level at E, let $\chi(S)dS$ be the conditional probability that the next energy level falls in the range $[E+S, E+S+dS]$ when the interval of length S contains no levels. Then, the nearest-neighbor spacing distribution is expressed as[41]

$$P(S)=\chi(S)\exp\left(-\int_0^S \chi(S')dS'\right), \tag{9}$$

where the exponential factor represents the probability that the interval of length S contains no levels. The Brody distribution comes from assuming that $\chi(S)$ is proportional to S^r:

$$P(S)=\frac{(1+r)\mu S^r}{D^{1+r}}\exp\left(-\mu\frac{S^{1+r}}{D^{1+r}}\right), \tag{10}$$

where

$$\mu=\left[\Gamma\left(\frac{(2+r)}{(1+r)}\right)\right]^{1+r}. \tag{11}$$

For r less than or equal to zero, Brody distributions exhibit level clustering, and for r greater than zero they exhibit level repulsion. The Poisson distribution and the Wigner distribution are the Brody distributions at $r=0$ and $r=1$, respectively.

The ratio of the fast component to the slow one, A_C/A_I, is estimated as[34]

$$\frac{A_C}{A_I}=\frac{2\Sigma\Sigma_{n<m}|a_n|^2|a_m|^2}{\Sigma_n|a_n|^4}\approx 1\Big/\sum_n |a_n|^4. \tag{12}$$

For the Bixon–Jortner (BJ) model, one finds that $1/\Sigma|a_n|^4$ is $2(\pi v/\varepsilon)^2$ at the limit of $v/\varepsilon \gg 1$. Since the number of s-character distributed states in the FWHM ΔE is estimated as $\Delta E/\varepsilon$, the value $2(\pi v/\varepsilon)^2$ can be regarded as the number of participating levels ($|s\rangle$ and the effectively coupled $|b_j\rangle$ levels). The ratio A_C/A_I thus provides the number of effectively coupled background levels, N_{eff}, which is defined in this paper as[42]

$$N_{\text{eff}}+1\equiv 1\Big/\sum_n |a_n|^4. \tag{13}$$

The meaning of N_{eff} is enriched by the observation that the time averaged probability of finding the system in $|s\rangle$ is, given the system being in $|s\rangle$ initially,[43–45]

$$P(s|s)\equiv\lim_{T\to\infty}\frac{1}{T}\int_0^T |\langle s|\Psi(t)\rangle|^2 dt=\sum_n |a_n|^4, \tag{14}$$

where we have used Eq. (3) neglecting all the relaxation constants. Since $P(s|s)$ can be interpreted to be inversely proportional to the phase space volume explored by the dynamics (in general, including electronic and spin degrees of freedom), the inverse of $P(s|s)$ is a measure of the number of participating states, i.e., $P(s|s)=1/(N_{\text{eff}}+1)$. The definition (13) can be rationalized in this way.

So far we have mentioned the three cases: (i) the BJ model (the level energies are perfectly correlated); (ii) the Poisson distribution (the energies are uncorrelated, randomly distributed); (iii) the Wigner distribution (the energies are correlated to some extent). In the time-dependent fluorescence signal, the three cases (i), (ii), and (iii) characteristically show the strong recurrence, biexponential decay, and the existence of correlation holes, respectively. If the correlation hole is difficult to experimentally detect, the decay is approximated by the biexponential form. The observed fluorescence decay can be explained by either case (ii) or case (iii); energy correlation is exaggerated in case (i). However, the meaning of N_{eff} remains the same and valid for any of the three cases. The two manifold BJ model will help us understand the magnetic field effect on ISC, since the effect can be discussed through N_{eff} (shown in Sec. II B). We adopt the two manifold BJ model in Sec. III to discuss the magnetic field effect while keeping in mind that energy correlation is overstated and randomness is completely thrown away.

B. Relation of N_{eff} with observables

It has been experimentally observed that as the applied magnetic field strength is increased the slow decay component of the fluorescence decreases in intensity while the fast component remains constant. For the moment, we attribute the magnetic quenching of the slow component to the efficient increase in N_{eff} by the magnetic field. A full detail of the mechanism is given in Secs. III–V.

The quantum yield of the slow component at zero field is given by time integration of the first term in Eq. (4):

$$\Phi_I(h_Z=0)=\frac{\Gamma_s}{\gamma_I(N_0+1)}, \tag{15}$$

where N_0 is the number of effectively coupled levels at zero field and h_Z represents the Zeeman interaction energy. Assuming that the s character is equally distributed among N_0+1 states, we have the average relaxation rate of eigenstates, γ_I,[4,34]

$$\gamma_I=(\gamma_s+N_0\gamma_T)/(N_0+1), \tag{16}$$

where γ_s is the relaxation rate of $|s\rangle$ and γ_T is the average relaxation rate of background levels. Substituting Eq. (16) into Eq. (15) yields

$$\Phi_I(h_Z=0)=\frac{\Gamma_s}{\gamma_s+N_0\gamma_T}. \tag{17}$$

At the high field limit, $N_{\rm eff}$ is expected to increase by a factor of the multiplicity M (for a triplet, $M=3$)

$$\Phi_I(h_Z=\infty)=\frac{\Gamma_s}{\gamma_s+MN_0\gamma_T}. \tag{18}$$

The quantum yield of the fast component is derived from the second term in Eq. (4) as

$$\Phi_C=\frac{\Gamma_s}{\Delta E}. \tag{19}$$

The fast component is independent of the field strength because the density of background states, $1/\varepsilon$, increases but the coupling v decreases.[20–24] The overall quantum yield Φ thus diminishes by the reduction in the slow component. In what follows we relate the three key factors, namely, the Zeeman energy, quantum yield, and $N_{\rm eff}$.

The value of h_Z where the reduction in quantum yield reaches one-half of the total amount of quenching at the high field limit may be employed as a measure of the efficiency in magnetic quenching. We denote it by $h_{1/2}$,

$$\begin{aligned}\Phi(h_Z=h_{1/2})&\equiv[\Phi(h_Z=0)+\Phi(h_Z=\infty)]/2\\ &\equiv\Phi_C+\Phi_I(h_Z=h_{1/2}),\end{aligned} \tag{20}$$

where $\Phi=\Phi_C+\Phi_I$. The definition of $h_{1/2}$ is thus reduced to

$$\Phi_I(h_Z=h_{1/2})=[\Phi_I(h_Z=0)+\Phi_I(h_Z=\infty)]/2. \tag{21}$$

Using Eqs. (17) and (18), one can rewrite Eq. (21) as

$$\frac{1}{\gamma_s+N_{1/2}\gamma_T}=\frac{1}{2}\left(\frac{1}{\gamma_s+N_0\gamma_T}+\frac{1}{\gamma_s+MN_0\gamma_T}\right), \tag{22}$$

where $N_{1/2}$ is the $N_{\rm eff}$ at $h_Z=h_{1/2}$. Rearranging the above equation, one finds that $N_{1/2}/N_0$ satisfies for $\gamma_T\neq 0$,

$$\frac{N_{1/2}}{N_0}=\frac{2MN_0\gamma_T+(M+1)\gamma_s}{(M+1)N_0\gamma_T+2\gamma_s}. \tag{23}$$

The $h_{1/2}$ can thus be defined as the Zeeman energy at which the $N_{\rm eff}$ satisfies Eq. (23). For $M=3$, the value of $N_{1/2}/N_0$ lies between 3/2 and 2 (according to whether $N_0\gamma_T>\gamma_S$ or $N_0\gamma_T<\gamma_S$). In Sec. IV we treat the right-hand side in Eq. (23) as practically constant: one can obtain $h_{1/2}$ without explicitly including the relaxation constants.

III. THE TWO MANIFOLD BIXON–JORTNER MODEL

In the absence of external field, a vibronic level in S_1, $|s\rangle$, is coupled to the manifold of rovibronic levels $\{|b_j\rangle\}$ that satisfy the $\Delta J=0$ selection rule (which are regarded as those arising from a spin sublevel potential surface). The effect of magnetic field on ISC is modeled by adding another background manifold $\{|c_j\rangle\}$ that is coupled to $\{|b_j\rangle\}$ by a magnetic field. The coupling scheme is illustrated in Fig. 2. Although a triplet electronic state has three spin sublevels, we deal with the two sublevel manifolds ($\{|b_j\rangle\}$ and $\{|c_j\rangle\}$) to draw the essence of the magnetic field effect. The model allows us to perform mathematical calculations easily and to derive useful analytical expressions.

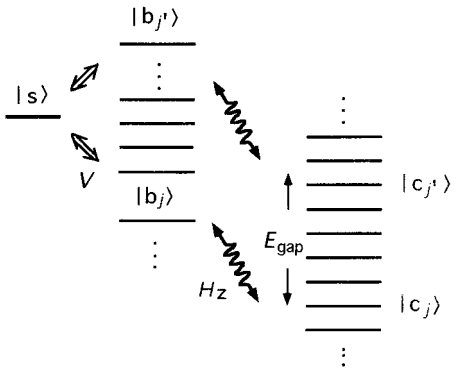

FIG. 2. Illustration of the two manifold model. In the absence of external field, a vibronic level in S_1, $|s\rangle$, is coupled to the rovibronic levels $\{|b_j\rangle\}$ that satisfy the selection rule $\Delta J=0$. The effect of magnetic field on ISC is modeled by adding another background manifold $\{|c_j\rangle\}$ that is coupled to $\{|b_j\rangle\}$ by the magnetic field. The arrows ($\Leftrightarrow$) and the wavy lines with arrow heads ($\leftrightsquigarrow$) indicate the intramolecular interaction V and the Zeeman interaction H_Z, respectively.

The total Hamiltonian for the system is written as

$$H=H_0+V+H_Z, \tag{24}$$

where H_Z is the Zeeman interaction and the unperturbed Hamiltonian H_0 gives the energies of the zero-order levels

$$H_0|s\rangle=E_s|s\rangle;\quad H_0|b_j\rangle=E_{bj}|b_j\rangle;\quad H_0|c_j\rangle=E_{cj}|c_j\rangle. \tag{25}$$

The absorption band shape (the distribution of absorption probability) and relevant quantities can be obtained by solving the eigenvalue problem (alternatively, one may employ the Green's function method)[46–49]

$$H|n\rangle=E_n|n\rangle. \tag{26}$$

The eigenfunctions $|n\rangle$ can be expressed as liner combinations of zero-order levels

$$|n\rangle=a_n|s\rangle+\sum_j b_{nj}|b_j\rangle+\sum_j c_{nj}|c_j\rangle. \tag{27}$$

Putting Eq. (27) into Eq. (26) and taking matrix elements with various zero-order states, one obtains the following set of equations:

$$(E_s-E_n)a_n+\sum_j\langle s|V|b_j\rangle b_{nj}=0, \tag{28a}$$

$$(E_{bj}-E_n)b_{nj}+\langle b_j|V|s\rangle a_n+h_Z c_{nj}=0, \tag{28b}$$

$$h_Z b_{nj}+(E_{cj}-E_n)c_{nj}=0, \tag{28c}$$

where $h_Z\equiv\langle b_j|H_Z|c_j\rangle$ and we have assumed that the spin sublevels of different rovibronic levels are not connected by the magnetic field (by assuming that the sublevel potentials are of the same form and shifted by $E_{\rm gap}$), that is,

$$\langle b_i|H_Z|c_j\rangle=\langle b_j|H_Z|c_j\rangle\delta_{ij}=h_Z\delta_{ij}, \tag{29}$$

$$E_{cj}=E_{bj}-E_{\rm gap}, \tag{30}$$

where $E_{\rm gap}$ is the zero-field splitting.

Substitution of Eqs. (28b) and (28c) into Eq. (28a) then leads to the characteristic equation for the eigenvalues

$$E_s - E_n + \sum_j \frac{|\langle s|V|b_j\rangle|^2}{E_n - E_{bj} - h_Z^2/(E_n - E_{cj})} = 0. \tag{31}$$

The total b and c components in the nth eigenstate, B_n and C_n, can be obtained from Eqs. (28b) and (28c):

$$B_n \equiv \sum_j b_{nj}^2 = a_n^2 \sum_j \frac{|\langle s|V|b_j\rangle|^2}{[E_n - E_{bj} - h_Z^2/(E_n - E_{cj})]^2}, \tag{32}$$

$$C_n \equiv \sum_j c_{nj}^2 = a_n^2 \sum_j \frac{h_Z^2 |\langle s|V|b_j\rangle|^2}{[(E_n - E_{bj})(E_n - E_{cj}) - h_Z^2]^2}. \tag{33}$$

The absorption probability of the eigenstate $|n\rangle$ is proportional to a_n^2. The value of a_n is determined from the normalization condition $a_n^2 + B_n + C_n = 1$:

$$a_n^2 = \left(1 + \sum_j \frac{|\langle s|V|b_j\rangle|^2 [(E_n - E_{cj})^2 + h_Z^2]}{[(E_n - E_{bj})(E_n - E_{cj}) - h_Z^2]^2} \right)^{-1}. \tag{34}$$

We here introduce the following assumptions as in the pioneering paper of Bixon and Jortner:[7]

(i) The background levels are equally spaced with an energy difference ε:

$$E_{bj} = j\varepsilon, \tag{35}$$

where $j = 0, \pm 1, \pm 2, \ldots$.

(ii) The matrix elements of the intramolecular interaction V are assumed to be a constant v, independent of the index j:

$$v = \langle s|V|b_j\rangle. \tag{36}$$

Under these assumptions, infinite summation in Eqs. (31)–(33) can be carried out. The characteristic Eq. (31) is reduced to

$$E_s - E_n + \frac{\pi v^2}{\varepsilon} [\cos^2 \theta \cot(\alpha - \beta) + \sin^2 \theta \cot(\alpha + \beta)] = 0, \tag{37}$$

where θ represents the degree of magnetic field-induced coupling between the two background manifolds

$$\theta = \frac{1}{2} \tan^{-1} \frac{2h_Z}{E_{\text{gap}}} \tag{38}$$

and α and β are defined as

$$\alpha = \pi \left(E_n + \frac{E_{\text{gap}}}{2} \right) \Big/ \varepsilon, \tag{39}$$

$$\beta = \pi \sqrt{E_{\text{gap}}^2 + 4h_Z^2}/(2\varepsilon). \tag{40}$$

Since α is a function of E_n, one must solve Eq. (37) numerically to get eigenvalues E_n. The absorption probability a_n^2 and the background components B_n and C_n are given by analytical forms

$$a_n^2 = \left[1 + \left(\frac{\pi v}{\varepsilon} \right)^2 [1 + \cos^2 \theta \cot^2(\alpha - \beta) + \sin^2 \theta \cot^2(\alpha + \beta)] \right]^{-1}, \tag{41a}$$

$$B_n = \left(\frac{\pi v}{2\varepsilon} \right)^2 a_n^2 \{ -\sin^2 2\theta [\cot(\alpha + \beta) - \cot(\alpha - \beta)]/\beta + (1 + \cos^2 2\theta)[\operatorname{cosec}^2(\alpha + \beta) + \operatorname{cosec}^2(\alpha - \beta)] + 2 \cos 2\theta [\operatorname{cosec}^2(\alpha + \beta) - \operatorname{cosec}^2(\alpha - \beta)] \}, \tag{41b}$$

$$C_n = \left(\frac{\pi v}{\varepsilon} \right)^2 \left(\frac{h_Z}{E_{\text{gap}}} \right)^2 a_n^2 \cos^2 2\theta \{ [\cot(\alpha + \beta) - \cot(\alpha - \beta)]/\beta + \operatorname{cosec}^2(\alpha + \beta) + \operatorname{cosec}^2(\alpha - \beta) \} \tag{41c}$$

which can be evaluated using the eigenvalues obtained.

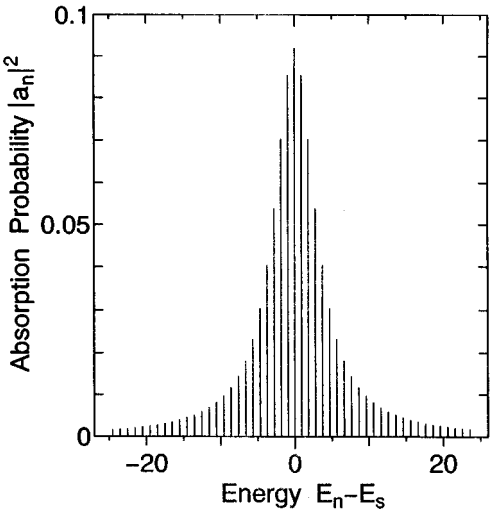

FIG. 3. Eigenvalues and absorption probabilities for the two manifold BJ model at zero field. The parameters used are: $v = \varepsilon = 1$, $E_{\text{gap}} = 10$, and $h_Z = 0$.

We now show some numerical examples (Figs. 3 and 4) for the eigenvalues and absorption probabilities. The Zeeman energies taken are in dimensionless units: $h_Z = 0$ in Fig. 3; (a) $h_Z = 10.3$ and (b) $h_Z = 10.077\,82$ in Fig. 4. The other parameters are the same for the three cases: $v = \varepsilon = 1$ and $E_{\text{gap}} = 10$. In the zero-field case (Fig. 3), the intensity profile (envelope) follows

$$A^0(E) \equiv \frac{v^2}{[(E - E_s)^2 + (\Delta E/2)^2]}, \tag{42}$$

where the FWHM ΔE at zero field is defined as

$$\Delta E = 2 \sqrt{v^2 + \left(\frac{\pi v^2}{\varepsilon} \right)^2} \approx 2\pi v^2/\varepsilon. \tag{43}$$

For $h_Z \neq 0$, it is evident that there exist *two* intensity profiles (sequences). In Fig. 4(a), a very intense profile and a very weak one exist; in Fig. 4(b), an intense one and a relatively weak one exist (the profile functions are plotted by dotted lines). We call the stronger one the ''strong sequence'' and the weaker one the ''weak sequence,'' though both can be comparable in intensity at high fields. The classification into the two sequences is artificial, but it helps our systematic understanding of the magnetic quenching.

The two profile functions can be obtained by rewriting Eq. (37) as

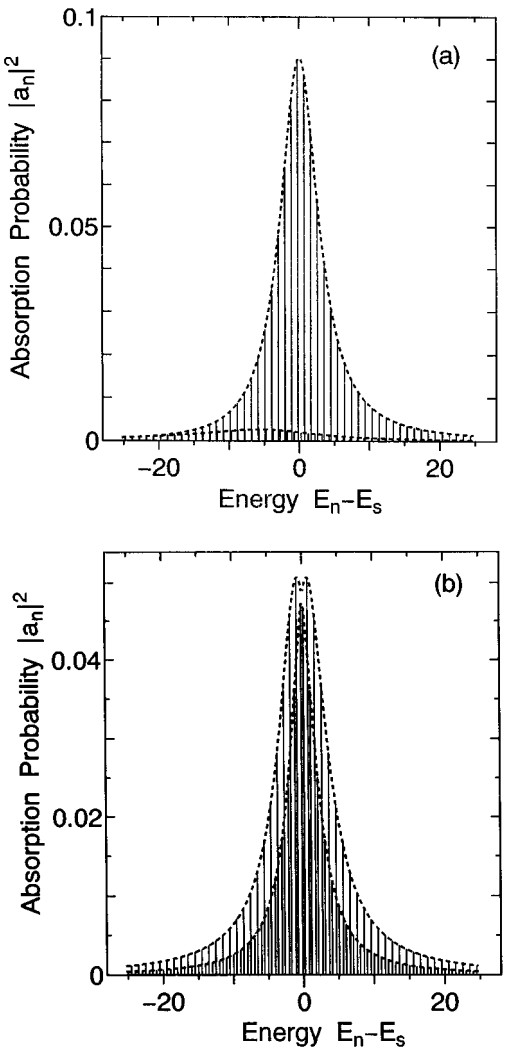

FIG. 4. Eigenvalues and absorption probabilities for the two manifold BJ model at (a) $h_Z=10.3$ and (b) $h_z=10.077\,82$. The other parameters are the same as in Fig. 3.

$$(X^2+4)\sin^2 2\alpha+4(2\cos 2\theta \sin 2\beta-X\cos 2\beta)\sin 2\alpha -X^2\sin^2 2\beta+4\cos^2 2\theta \sin^2 2\beta -4X\cos 2\theta \sin 2\beta \cos 2\beta=0, \tag{44}$$

where

$$X=\frac{2\varepsilon(E_n-E_s)}{\pi v^2}. \tag{45}$$

Since Eq. (44) is a quadratic equation for $\sin 2\alpha$, we have two sets of solutions yielding the strong and weak sequences (a pair of characteristic equations for determining the eigenvalues)

$$\sin 2\alpha = \frac{-2(2\cos 2\theta \sin 2\beta-X\cos 2\beta)\pm\sqrt{X^2 f(\theta,\beta,X)}}{X^2+4}, \tag{46}$$

where

$$f(\theta,\beta,X)\equiv X^2\sin^2 2\beta+4X\cos 2\theta \sin 2\beta\cos 2\beta +4(1-\cos^2 2\theta \sin^2 2\beta). \tag{47}$$

The corresponding $\cos 2\alpha$ are also obtained by deriving the quadratic equation for $\cos 2\alpha$ from Eq. (37):

$$\cos 2\alpha = \frac{-X(2\cos 2\theta \sin 2\beta-X\cos 2\beta)\mp 2\sqrt{f(\theta,\beta,X)}}{X^2+4}. \tag{48}$$

The signs of the square roots in Eqs. (46) and (48) are, for $X>0$, combined in order of appearance and, for $X<0$, in reverse order. The $\sin 2\alpha$ and $\cos 2\alpha$ are regarded as functions of ''continuous'' X. The profiles of a_n^2, B_n, and C_n for the strong and weak sequences can therefore be obtained as functions of continuous energy E_n-E_s by substituting $\sin 2\alpha$ and $\cos 2\alpha$ into Eqs. (41). The $\cot(\alpha+\beta)$ and $\cot(\alpha-\beta)$ in Eqs. (41) are related with $\sin 2\alpha$ and $\cos 2\alpha$ as follows:

$$\cot(\alpha\pm\beta)=\frac{\cot\alpha\cot\beta\mp 1}{\cot\beta\pm\cot\alpha}, \tag{49}$$

$$\cot\alpha=\frac{1+\cos 2\alpha}{\sin 2\alpha}. \tag{50}$$

IV. NUMERICAL RESULTS AND DISCUSSION

The two cases (a) and (b) in Fig. 4 remarkably differ in the number $N_{\rm eff}$, although the field strengths are nearly equal. They are understood as extreme cases and classified by using the eigenfunctions for the Hamiltonian H_0+H_Z (excluding V). There are two sets of eigenstates (field dressed states) for this Hamiltonian

$$|\hat{b}_j\rangle=\cos\theta\,|b_j\rangle+\sin\theta\,|c_j\rangle;$$
$$|\hat{c}_j|=-\sin\theta\,|b_j\rangle+\cos\theta\,|c_j\rangle. \tag{51}$$

The corresponding eigenvalues for the two sets $\{|\hat{b}_j\rangle\}$ and $\{|\hat{c}_j\rangle\}$ are given by

$$\hat{E}_{bj}=\frac{E_{bj}+E_{cj}+\hat{E}_{\rm gap}}{2};\quad \hat{E}_{cj}=\frac{E_{bj}+E_{cj}-\hat{E}_{\rm gap}}{2}, \tag{52}$$

where $\hat{E}_{\rm gap}$ denotes the energy difference between the dressed states $|\hat{b}_j\rangle$ and $|\hat{c}_j\rangle$:

$$\hat{E}_{\rm gap}=\sqrt{E_{\rm gap}^2+4h_Z^2}. \tag{53}$$

The eigenvalues of the field dressed states shift with h_Z (the level spacings in the same manifold remain constant).

The two extreme cases can be interpreted as the following two cases of the dressed state energy structure. (a) The eclipsed structure: $\hat{E}_{\rm gap}=l\varepsilon$ where l is an integer, i.e., the two sets of dressed states overlap in energy [cf. Fig. 5(a)]. Since $\beta=\hat{E}_{\rm gap}\pi/2\varepsilon$, $\beta=\pi l/2$. (b) The staggered structure: $\hat{E}_{\rm gap}=(l+1/2)\varepsilon$ or $\beta=\pi\ (l+1/2)/2$, i.e., the two sets of dressed states are staggered so that the nearest-neighbor level spacing of dressed states is $\varepsilon/2$ [cf. Fig. 5(b)].

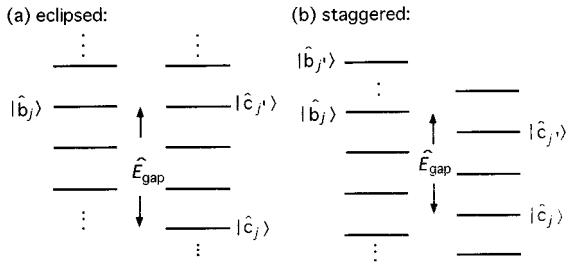

FIG. 5. The two extreme cases of the energy structure of field dressed states: (a) the eclipsed structure and (b) the staggered structure. In the eclipsed structure, the two sets $|\hat{b}_j\rangle\}$ and $\{|\hat{c}_j\rangle\}$ of dressed states overlap in energy and in the staggered structure the two sets of dressed states are staggered so that the nearest-neighbor level spacing of dressed states is $\varepsilon/2$.

Figure 4(a) corresponds nearly to the eclipsed structure and Fig. 4(b) corresponds to the staggered structure. The eclipsed and staggered structures alternatively appear at intervals of about $\varepsilon/2$ in h_Z.

A. The eclipsed structure

In this case the fine structure of the absorption band is the same as in the zero-field case [cf. Figs. 3 and 4(a)], irrespective of the field strength. The number of effectively coupled background levels remains unchanged even at high fields [$h_Z/E_{\rm gap}>1$ in Fig. 2(a)]. Mathematically it is easy to show that the absorption probability [Eq. (41a)] is classified into two sets $\{a_n^2=0\}$ and $\{a_n^2(h_Z=0)=A^0(E_n)\}$ by putting $\beta=\pi l/2$ into Eqs. (46) and (48).

The reason is elucidated as follows. Take a pair of degenerate dressed states $|\hat{b}_j\rangle$ and $|\hat{c}_{j'}\rangle$ as shown in Fig. 5(a) (j' is chosen so that its energy $\hat{E}_{cj'}$ is equal to $\hat{E}_{bj}$). Since these two states have the same energy, a unitary transformation of them also leads to a diagonal representation of H_0+H_Z (for any value of η)

$$\begin{aligned}|\phi_0\rangle &\equiv \sin\,\eta\,|\hat{b}_j\rangle+\cos\,\eta\,|\hat{c}_{j'}\rangle\\ &=\sin\,\eta\,\sin\,\theta\,|c_j\rangle+\cos\,\eta\,\cos\,\theta\,|c_{j'}\rangle\\ &\quad+\sin\,\eta\,\cos\,\theta\,|b_j\rangle-\cos\,\eta\,\sin\,\theta\,|b_{j'}\rangle \qquad (54)\end{aligned}$$

and

$$\begin{aligned}|\phi_1\rangle &\equiv \cos\,\eta\,|\hat{b}_j\rangle-\sin\,\eta\,|\hat{c}_{j'}\rangle\\ &=\cos\,\eta\,\cos\,\theta\,|b_j\rangle+\sin\,\eta\,\sin\,\theta\,|b_{j'}\rangle\\ &\quad+\cos\,\eta\,\sin\,\theta\,|c_j\rangle-\sin\,\eta\,\cos\,\theta\,|c_{j'}\rangle. \qquad (55)\end{aligned}$$

It is possible to determine the parameter η so that $\langle s|V|\phi_0\rangle=0$. The series of $|\phi_0\rangle$ can be chosen not to interact with $|s\rangle$ (in the present case $\eta=\theta$). On the other hand, in the series of $|\phi_1\rangle$, the dressed states are equally spaced, equally coupled to $|s\rangle$ (the spacing is ε and the coupling constant is v) as in the zero-field case. The total volume in phase space increases at high fields by a factor of 2 but the actual dynamics explores only half of it.

That the energy structure of the absorption band is unchanged does not mean that the zero-order manifold $\{|c_j\rangle\}$ is insulated in the dynamics. It means that the time evolution of the $|s\rangle$ level population behaves as in the zero-field case but does not mean that $\{|b_j\rangle\}$ and $\{|c_j\rangle\}$ are uncoupled [see Eq. (55)]. The phase space *volume* explored is the same as in the zero-field case but the region explored is different. The mixing ratio C_n/B_n in $|\phi_1\rangle$ is

$$\frac{C_n}{B_n}=\frac{2\,\sin^2\,\theta\,\cos^2\,\theta}{\cos^4\,\theta+\sin^4\,\theta} \qquad (56)$$

which is independent of $|n\rangle$. The coupling between the zero-order manifolds is enhanced in comparison with that evaluated from the coefficients of b and c components in $|\hat{b}_j\rangle$, i.e., $C_n/B_n=\sin^2\,\theta/\cos^2\,\theta$. At low fields ($h_Z/E_{\rm gap}<1$), the value given by Eq. (56) is twice as large as $\sin^2\,\theta/\cos^2\,\theta$.

When two dressed states are degenerate, it is always possible, irrespective their coupling strengths (even if the coupling strength fluctuates), to find a transformation under which one state carries coupling strength to $|s\rangle$ and the other does not. By setting the condition $\langle s|V|\phi_0\rangle=0$ in Eq. (54), one finds

$$\tan\,\eta=\frac{\sin\,\theta}{\cos\,\theta}\frac{\langle s|V|b_{j'}\rangle}{\langle s|V|b_j\rangle}.$$

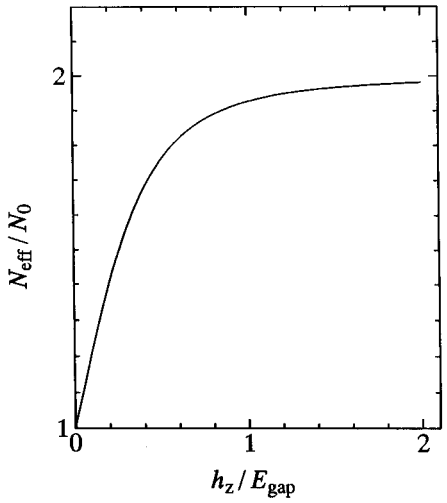

FIG. 6. The relation between $N_{\rm eff}/N_0$ and $h_Z/E_{\rm gap}$ for the staggered structure. The N_0 is assumed to be large ($v/\varepsilon\gg1$).

B. The staggered structure

The staggered structure changes the situation. In Fig. 4(b), $N_{\rm eff}$ is twice as large as N_0. If the level structure is restricted to the staggered case, $N_{\rm eff}/N_0$ increases with increasing $h_Z/E_{\rm gap}$ as shown in Fig. 6 (for $v/\varepsilon\gg1$). Since the level structure depends on h_Z, we have continuously changed the h_Z while keeping the structure staggered, i.e., setting $\beta=\pi\,(l+1/2)/2$. The value of $h_{1/2}$ can be determined as follows. For the multiplicity $M=2$, the right-hand side in Eq. (23) can take values between 4/3 and 3/2. We treat the value as a constant 3/2: $h_{1/2}$ is defined as the Zeeman energy at which $N_{\rm eff}$ is one-and-a-half times as large as the zero-field value N_0. We have numerically checked that N_0 is nearly independent of E_s and is regarded as a function of the ratio v/ε only [calculate Eq. (13)]. It is found that at the limit of $v/\varepsilon\gg1$ the value N_0+1 becomes $2(\pi v/\varepsilon)^2$ [insert Eq. (42) into Eq. (13) and replace summation with integration]. We

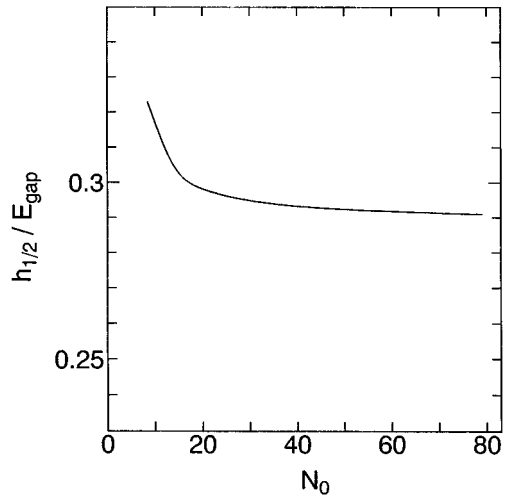

FIG. 7. The relation between $h_{1/2}/E_{\rm gap}$ and N_0 for the staggered structure. The $h_{1/2}$ have been obtained by setting $N_{1/2}/N_0=3/2$ [see Eq. (23)].

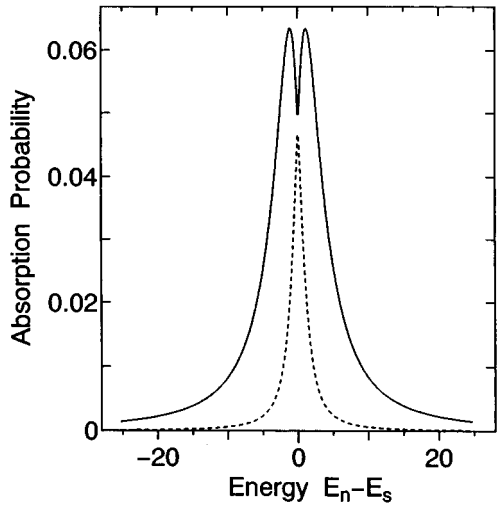

FIG. 9. The envelopes of absorption probabilities for the strong and weak sequences. The parameters used are: $h_Z=2.839\,45$, $E_{\rm gap}=10.0$, and $\nu=\epsilon=1$. The solid line represents the envelope A^+ of the strong sequence and the dotted line represents the envelope A^- of the weak sequence.

have also noted that $N_{\rm eff}$ is a function of two ratios ν/ε and $h_Z/E_{\rm gap}$ [cf. Eqs. (41a) and (46)–(50)]. The ratio $h_{1/2}/E_{\rm gap}$ is therefore determined by ν/ε (or N_0) alone. The relation, shown in Fig. 7, is obtained numerically by finding the h_Z at which $N_{1/2}/N_0$ becomes 3/2.

The result suggests the possibility that the ratio $h_{1/2}/E_{\rm gap}$ can be much smaller than 1. The curve however does not agree with the experimentally observed tendency that $h_{1/2}$ *drastically* decreases with increasing N_0. The magnetic quenching depends strongly on the vibrational level density of the triplet state coupled to S_1 (i.e., on N_0). For instance, in magnetic quenching of pyrimidine, the half-quenching field strength $H_{1/2}$ for $6a^2$ of S_1 is less than one-third of that of $6a^1$ (the energy difference between the two levels is about 600 $\rm cm^{-1}$).[21] The magnetic quenching also becomes more efficient with increasing rotational quantum number J' of the excited level. In Fig. 8, $H_{1/2}$ on 0–0 band excitation for pyrazine (■) and pyrazine-d_4 (○) are plotted against $2J'+1$.[20,22] The drastic decrease in $H_{1/2}$ implies that N_0 is nearly proportional to $2J'+1$. It is probable that K scrambling in the triplet caused by Coriolis interaction leads to the selection rule $\Delta K=$anything (the breakdown of the symmetric top approximation may also be responsible for it).[50–53]

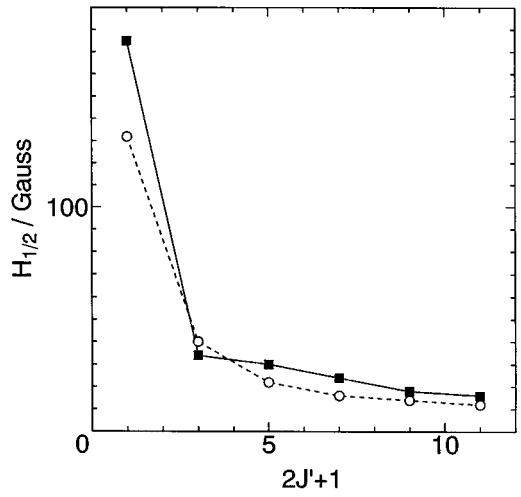

FIG. 8. Half-quenching field strengths $H_{1/2}$ on 0–0 band excitation for pyrazine (■) and pyrazine-d_4 (○). They are plotted against $2J'+1$.

We examine why it is not necessary for $h_{1/2}$ to be as large as $E_{\rm gap}$. The disagreement about the dependence of $h_{1/2}$ on N_0 will be discussed in detail in Sec. V. As shown in Fig. 4(b), the absorption band contains the strong sequence and the weak sequence. Another example is given in Fig. 9 for $h_Z/E_{\rm gap}=2.839\,45$ ($E_{\rm gap}=10.0$). The solid line represents the envelope A^+ of the strong sequence and the dotted line represents the envelope A^- of the weak sequence. It is found that the sum of the two envelopes is nearly equal to the zero-field envelope $A^0(E)$, irrespective of the field strength

$$A^+(E)+A^-(E)\approx A^0(E) \tag{57}$$

which means that the decay rate of the fast component remains unchanged. This is the case for high rotational or vibrational levels of S_1. For such levels, N_0 is expected to be large and the band envelope smoothed (the s-character distribution locally averaged for small energy intervals) is expected to be Lorentzian. If the magnetic field increases the density of states effectively by a factor of 3, the coupling strength v^2 decreases by a factor of 3 (for $M=3$).

We have found that the envelope of the weak sequence is well approximated by

$$A^-(E)\approx \frac{v^2\,\sin^2\,\theta}{[(E-E_s)^2+2(\Delta E/2)^2\,\sin^2\,\theta]} \tag{58}$$

and therefore the strong sequence is well approximated by

$$A^+(E)\approx A^0(E)-A^-(E). \tag{59}$$

Equation (58) indicates that the envelope of the weak sequence has FWHM of $\sqrt{2}\Delta E|\sin\theta|$ and height of $2(v/\Delta E)^2$ ($\approx 1/N_0$). The width increases linearly with $h_Z/E_{\rm gap}$ at low fields but the height, which is independent of the field strength and a half of the height A^0 ($E=E_s$) at *zero field*, is

nonzero even at zero field. This suggests that even at low fields there are chances of fitting eigenstates into the envelope and the magnetic field is more operative than usually expected from the magnitude of the mixing coefficient $\sin^2\theta$.

For large N_0, summation in Eq. (13) can be replaced with integration and only the area of the envelope squared A^2 matters

$$\frac{N_{\text{eff}}+1}{N_0+1} \approx \frac{\Sigma_{n \text{ for } h_Z=0}[A^0(E_n)]^2}{\Sigma_{\text{strong}}[A^+(E_n)]^2+\Sigma_{\text{weak}}[A^-(E_n)]^2} \approx \frac{\int[A^0(E)]^2dE}{\int[A^+(E)]^2dE+\int[A^-(E)]^2dE} = \frac{1}{1-|\sin\theta|[4(1-\sqrt{2}|\sin\theta|)/\cos 2\theta-1]/\sqrt{2}}, \tag{60}$$

where the strong and weak under summation symbols denote the eigenvalues belonging to the strong sequence and those to the weak sequence, respectively. The curve in Fig. 6 is identical with Eq. (60). The asymptotic value in Fig. 7 corresponds to the approximate value $\sqrt{17}/16 \approx 0.26$ obtained by setting the last version in Eq. (60) equal to 3/2. As expected, the last version becomes 2 as $h_Z/E_{\text{gap}} \to \infty$. [The ratio in area between the two sequences, $\int A^-(E)dE/\int A^+(E)dE$, is estimated to be $\sqrt{2}|\sin\theta|/(2-\sqrt{2}|\sin\theta|)$ by using Eqs. (58) and (59).] Equation (60) means, as shown in Fig. 7, that the ratio N_{eff}/N_0 can be regarded as a function of h_Z/E_{gap} only and independent of N_0. In what follows we will reveal how the magnetic field couples zero-order levels and why it distributes s character over many eigenstates so efficiently.

We go over the degree of mixing between the two zero-order manifolds $\{|b_j\rangle\}$ and $\{|c_j\rangle\}$ for each sequence. Figure 10(a) shows the envelopes of a_n^2, B_n, and C_n values in the strong sequence and Fig. 10(b) shows those in the weak sequence. The B_n envelopes are indicated by broken lines and the C_n envelopes are indicated by dotted lines. The s-component envelopes are indicated by solid lines [they are approximated by the envelope functions (58) and (59)]. The parameters are the same in Fig. 9. For the strong sequence, the b component dominates over the c component but the degree of mixing depends on the eigenvalue. In the far wing regions ($|E_n-E_s| \gg \Delta E$), the mixing is as small as expected from the coefficients of b and c components in $|\hat{b}_j\rangle$ [see Eq. (51)]; the ratio $B_n:C_n$ is given by $\cos^2\theta:\sin^2\theta$ (0.935:0.065). However, as the energy approaches the center of the absorption band, the c component grows while the b component diminishes; at the absorption band center the zero-order manifolds are fully mixed in terms of subtotal population, i.e., the ratio $B_n:C_n$ is 1:1. For the weak sequence, the majority is reversed (the major component is c and the minor component is b) but the main feature remains the same. In the far wing regions, the mixing is small and given by the coefficients of b and c components in $|\hat{c}_j\rangle$, i.e., $B_n:C_n=\sin^2\theta:\cos^2\theta$. At the center of the absorption band, the zero-order manifolds are fully mixed.

It is interesting to know how many zero-order levels are involved in an eigenstate. The number of zero-order b levels

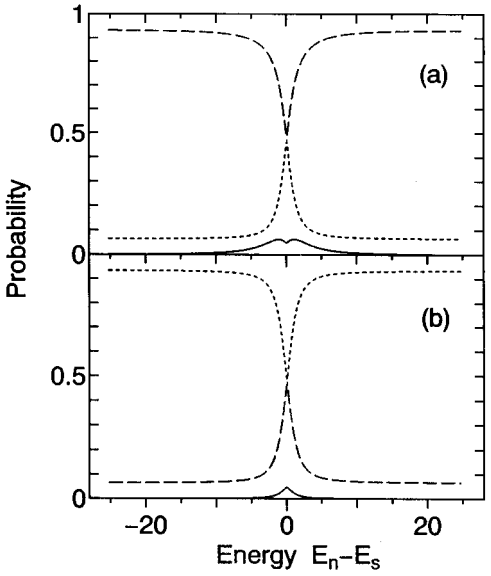

FIG. 10. The envelopes of the zero-order components a_n^2, B_n, and C_n for (a) the strong sequence and (b) the weak sequence. The B_n envelopes are indicated by broken lines and the C_n envelopes are indicated by dotted lines. The s-component envelopes are indicated by solid lines. The parameters are the same as in Fig. 9.

(or c levels) involved in an eigenstate $|n\rangle$, N_B (or N_c), may be defined as

$$N_B=\frac{(\Sigma_j b_{nj}^2)^2}{\Sigma_j b_{nj}^4}; \quad N_C=\frac{(\Sigma_j c_{nj}^2)^2}{\Sigma_j c_{nj}^4}, \tag{61}$$

where the numerators are necessary to take into account the norm of each component. Figure 11(a) shows the envelopes of these values in the strong sequence and Fig. 11(b) shows those in the weak sequence. The broken lines denote N_B and the dotted lines denote N_C. Roughly speaking, as the eigenstate lies closer to the band center, the number of zero-order

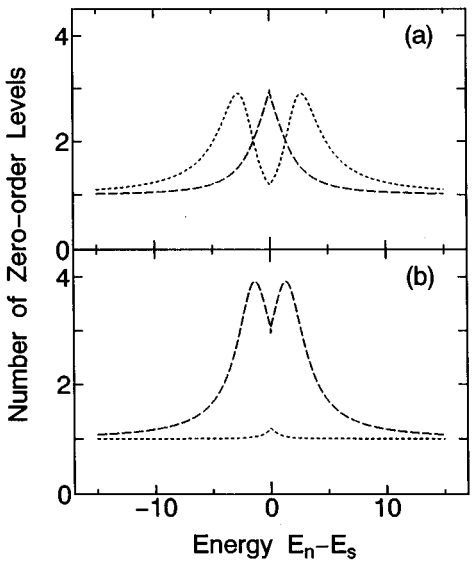

FIG. 11. The number of zero-order b levels (N_B) and that of zero-order c levels (N_C) for (a) the strong sequence and (b) the weak sequence. The broken lines denote N_B and the dotted lines denote N_C. The parameters are the same as in Fig. 9.

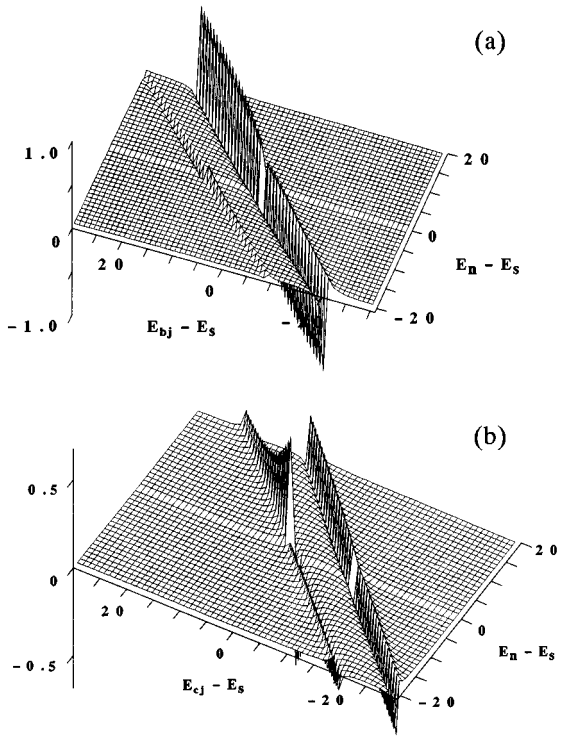

FIG. 12. Zero-order components in eigenstates $|n\rangle$ for the strong sequence: (a) the coefficient of $|b_j\rangle$, i.e., $\{b_{nj}\}$ and (b) the coefficient of $|c_j\rangle$, i.e., $\{c_{nj}\}$, are given as functions of the eigenvalue E_n-E_s and the zero-order level energy $E_{bj}-E_s$ or $E_{cj}-E_s$.

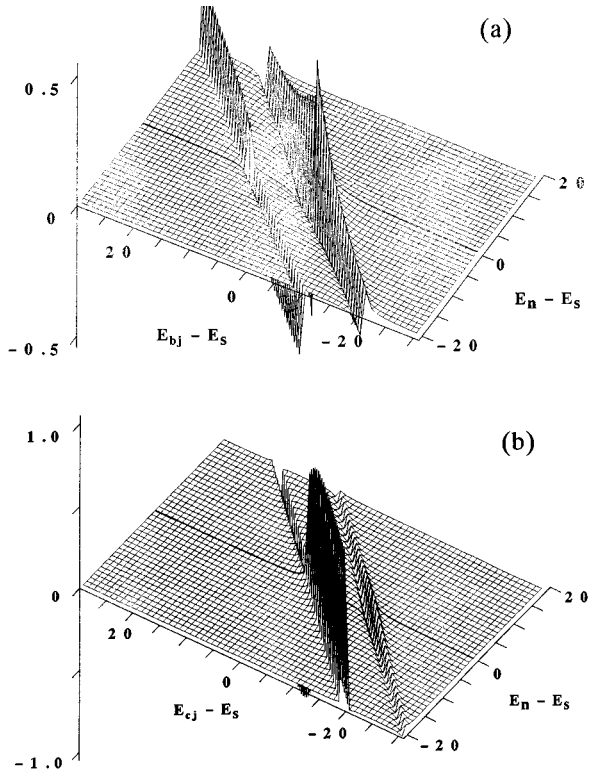

FIG. 13. Zero-order components in eigenstates $|n\rangle$ for the weak sequence: (a) the coefficient of $|b_j\rangle$, i.e., $\{b_{nj}\}$ and (b) the coefficient of $|c_j\rangle$, i.e., $\{c_{nj}\}$.

levels involved increases (which means more "ergodic").[43,44] The fact that N_B in the weak sequence increases near the band center, shown in Fig. 11(b), indicates that the growth of the weak sequence near the band center is accompanied with mixing among nearby $|b\rangle$ and $|c\rangle$ levels. The increase in N_B in the strong sequence, shown in Fig. 11(a), is due to intramanifold (b-manifold) mixing via the $|s\rangle$ level which takes place at zero field (qualitatively, the N_B in the strong sequence changes with energy as in the zero-field case).

At this stage we briefly summarize the mixing scheme and the mechanism of the growth of N_{eff}. In the far wing regions, the field dressed states $\{|\hat{b}_j\rangle\}$ and $\{|\hat{c}_j\rangle\}$ are approximate eigenstates of the total Hamiltonian H. The former set corresponds to the strong sequence and the latter set corresponds to the weak sequence. The mixing between the two levels $|b_j\rangle$ and $|c_j\rangle$ in a field dressed state is weak, i.e., $B_n:C_n=\cos^2\theta:\sin^2\theta$ for the strong sequence, and $\sin^2\theta:\cos^2\theta$ for the weak sequence. In the far wing regions, an eigenstate contains only one b-character level and only one c-character level (a pair of levels connected by the Zeeman interaction). On the other hand, near the absorption band center, inter- and intramanifold mixings are accelerated, that is, N_B and N_C increase, which concurrently distributes the s character to more eigenstates. (Here "intermanifold" means "between the b and c manifolds" and "intramanifold" means "among levels of the b manifold" or "among levels of the c manifold.") This is an explanation for the growth of the weak sequence. One may also say that the presence of the doorway $|s\rangle$ level (or the $s-b$ intramolecular interaction V) distributes the b and c characters more efficiently (than in the presence of a magnetic field alone) by distributing itself over nearby eigenstates.

We next make the above summary more tangible by calculating coefficients of $|b_j\rangle$ and $|c_j\rangle$ in eigenstates $|n\rangle$, i.e., $\{b_{nj}\}$ and $\{c_{nj}\}$. The coefficients for the strong and weak sequences are plotted in Figs. 12 and 13, respectively. They are given as functions of the the eigenvalue E_n-E_s and the zero-order level energy $E_{bj}-E_s$ or $E_{cj}-E_s$. Figures 12(a) and 13(a) show b coefficients $\{b_{nj}\}$ and Figs. 12(b) and 13(b) show c coefficients $\{c_{nj}\}$. The mechanism of zero-order level scrambling can be visualized by the coupling scheme drawn in Fig. 2.

At zero field, there are no intermanifold mixings; the only existing mixing is the intramanifold one induced by V. The interaction V scrambles b_j levels lying in the range ΔE around E_s. The intramanifold mixing existing at zero field, which we will call V-induced intramanifold mixing, is responsible for the nonzero b coefficients along the $E_{bj}=E_n$ line in Fig. 12(a). In the far wing regions the positive part of $\{b_{nj}\}$ exceeds the negative part overwhelmingly, or vice versa, that is, $N_B=1$. As the eigenvalue approaches E_s the positive and negative parts become comparable: the N_B increases as shown in Fig. 11(a).

The Zeeman interaction induces intermanifold mixing. It connects the same vibronic levels $\{b_j$ and $c_j\}$ belonging to different manifolds (H_Z-induced sublevel mixing). For the strong sequence, as expected from the scheme in Fig. 2, this sublevel mixing creates nonzero c coefficients along the line

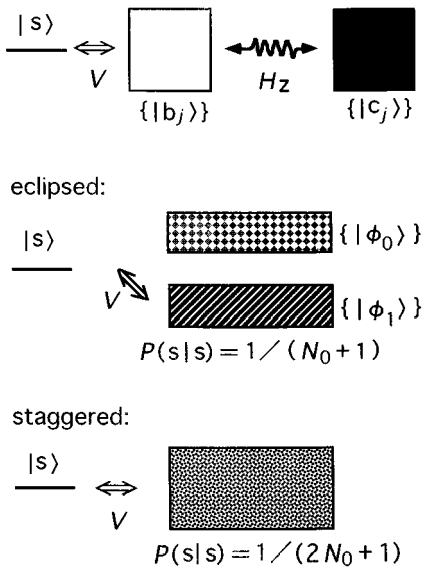

FIG. 14. The accessible phase spaces for the eclipsed and staggered structures. The top represents the sequential coupling scheme. The arrow ($\Leftrightarrow$) denotes the intramolecular interaction V that couples the doorway level $|s\rangle$ to the b manifold and the wavy line ($\leftrightsquigarrow$) denotes the Zeeman interaction H_Z that couples the b manifold to the c manifold. The size of a box represents the phase space volume of the manifold (the white area represents b component and the black area represents c component). The eclipsed structure converts the sequential coupling scheme to that in the middle, where only half of the overall phase space is accessible from $|s\rangle$. The accessible region is described by $\{|\phi_1\rangle\}$ and the inaccessible region is described by $\{|\phi_0\rangle\}$ [see Eqs. (54) and (55)]. Each phase space volume is identical with that of the b manifold. Therefore, the time-averaged probability of finding the system in $|s\rangle$, $P(s|s)$, remains unchanged, i.e., $P(s|s)=1/(N_0+1)$. For the staggered structure case, illustrated at the bottom, all the phase space is accessible at high fields. The probability $P(s|s)$ can be reduced to $1/(2N_0+1)$.

at $E_{cj}=E_n-E_{\rm gap}$ [Fig. 12(b)]. The nonzero b coefficients along the $E_{bj}=E_n$ line in Fig. 12(a) indicate the companion (parent) b levels (these eigenstates are b-character dominated). For the weak sequence, the eigenstates are c-character dominated. The b levels appearing along the line at $E_{bj}=E_n+E_{\rm gap}$ in Fig. 13(a) are paired by H_Z with the parent c levels appearing along the $E_{cj}=E_n$ line in Fig. 13(b).

There is nothing new about the mixings we have mentioned in the above two paragraphs. New types of inter- and intramanifold mixings are induced by the coexistence of the intramolecular interaction and the magnetic field. In the following we give a full detail of them.

1. Isoenergetic intermanifold mixing

There is no direct interaction between b_j and $c_{j'}$ (the chain of existing interactions is like $b_j \Leftrightarrow s \Leftrightarrow b_{j'} \leftrightsquigarrow c_{j'}$ in Fig. 2), but isoenergetic paths are opened up between the zero-order manifolds. The fact that in the weak sequence [Fig. 13(a)] nonzero b coefficients appear at the $E_{bj}=E_n$ line indicates that a zero-order c level can be mixed up with b levels that are energetically near the c level. This type of mixing indirectly couple, say, $|b_j\rangle$ and $|c_{j'}\rangle$ in Fig. 2. This is a novel type of mixing we have never realized before. The key process is the Raman-like second-order one $s \Leftrightarrow b_{j'} \leftrightsquigarrow c_{j'}$ which supplies s character to the zero-order $c_{j'}$ level.[54] The resulting state is entitled to interact with isoenergetic $\{b_j\}$ levels through V. One may say that the $|s\rangle$ level triggers isoenergetic mixing between zero-order manifolds.

On the basis of second-order perturbation theory the s component in a c-character dominated eigenstate is estimated by $|vh_Z/E_{\rm gap}(E_s-E_{cj})|^2$, which explains the feature of the weak sequence that as the eigenvalue ($\approx E_{cj}$) approaches E_s the s and b components increase. This expression is identical with the second-order expansion form of the envelope function A^- [see Eq. (58)], indicating that the Raman-like process is the key one. As shown in Fig. 13(a), in the far wing regions the b component comes mainly from the $E_{\rm gap}$ shifted b level connected by H_Z-induced sublevel mixing; in the center, however, the main b component comes from isoenergetic b levels [cf. Fig. 10(b)]. A reverse flow is also generated by the isoenergetic intermanifold mixing; it renders c character to the b-character dominated state. It is shown in Fig. 12(b) that nonzero c coefficients appear at the isoenergetic line $E_{cj}=E_n$. This type of component grows as the eigenvalue gets closer to E_s. It is generally concluded that in the center of the absorption band the main b (or) c levels included in an eigenstate are isoenergetic ones and not the $E_{\rm gap}$ shifted ones. The $E_{\rm gap}$ shifted b levels render s character to the zero-order c levels and mediate between isoenergetic b and c levels. The role of the $E_{\rm gap}$ shifted level is important in isoenergetic intermanifold mixing but it is ''catalytic'' in that near the band center the $E_{\rm gap}$ shifted level decreases in population.

2. Intramanifold mixing between gap separated levels

Nonzero b and c coefficients exist at $E_{bj}=E_n+E_{\rm gap}$ in Fig. 12(a) and at $E_{cj}=E_n-E_{\rm gap}$ in Fig. 13(b), respectively. They are virtually regarded as mixings between intramanifold levels separated by $E_{\rm gap}$. One may interpret the mixing as a virtual second-order perturbation of the Zeeman interaction and the isoenergetic intermanifold mixing. For instance, nonzero components at $E_{bj}=E_n+E_{\rm gap}$ in Fig. 13(a) are induced by processes such as $b_{j'} \leftrightsquigarrow c_{j'} \leftrightarrow b_j$ (the arrow $\leftrightarrow$ indicates the isoenergetic intermanifold mixing). This type of virtual second-order process is fourth order in real perturbation: the intramanifold mixing between gap separated levels is the smallest.

C. Results obtained from the two manifold Bixon–Jortner model

We have examined two extreme energy structures, namely, the eclipsed and staggered structures. Between the two cases there is a major difference; with increasing field strength the $N_{\rm eff}$ increases for the staggered structure but remains unchanged for the eclipsed structure. The difference can be schematically illustrated by coupling schemes in Fig. 14. The top represents the sequential coupling scheme. The arrow ($\Leftrightarrow$) denotes the intramolecular interaction V that couples the doorway level $|s\rangle$ to the manifold $\{|b_j\rangle\}$ and the wavy line ($\leftrightsquigarrow$) denotes the Zeeman interaction H_Z that couples the manifold $\{|b_j\rangle\}$ to $\{|c_j\rangle\}$. The size of a box represents the phase space volume of the manifold (which should be taken relative). The eclipsed structure converts the

sequential coupling scheme to that in the middle, where only half of the overall phase space ($\{|b_j\rangle\}$ and $\{|c_j\rangle\}$) is accessible from $|s\rangle$. The accessible region is described by $\{|\phi_1\rangle\}$ and the inaccessible region is described by $\{|\phi_0\rangle\}$ [see Eqs. (54) and (55)]. Each phase space volume is identical with that of $\{|b_j\rangle\}$. Therefore, the time averaged probability of finding the system in $|s\rangle$, $P(s|s)$, remains unchanged, i.e., $P(s|s)=1/(N_0+1)$. The feature that $N_{\rm eff}$ remains the same is independent of the magnetic field strength. On the other hand, for the staggered structure, all the phase space is accessible at high fields. The probability $P(s|s)$ can be reduced to $1/(2N_0+1)$.

What the staggered structure model suggests is in accord with experimental results on the magnetic quenching. Of special importance are the Raman-like *s*-character transfer to indirectly coupled background levels, concurrent isoenergetic intermanifold mixing, and resultant weak sequence. They are unique to the energy transfer among three or more manifolds and are the keys to understanding the reason why the efficiency of magnetic quenching is so high at anomalously low fields. For the eclipsed structure model, which explains nothing with the magnetic quenching, the Raman-like process is not operative. The energy correlation between the two *dressed* state manifolds $\{|\hat{b}_j\rangle\}$ and $\{|\hat{c}_j\rangle\}$ prevents a weak sequence from growing with increasing H_Z.

At any field strength, there is a chance that a $|\hat{b}\rangle$ dressed state energetically coincides with a $|\hat{c}\rangle$ state. The problem is that if a perfect staggered structure is impossible even a very high field will not reduce the quantum yield to 1/2 (for $M=2$) of the zero-field value contrary to the experimental fact. Necessary conditions for the complete magnetic quenching (that the quantum yield is reduced to 1/2 at high fields) are: (i) the energy distribution of dressed states at high fields is the same type as that of the *b* manifold and the average spacing is reduced to $\varepsilon/2$; (ii) the coupling distribution at high fields is the same type of that of the *b* manifold and the rms of the coupling is reduced to $(\overline{v_j^2})^{1/2}/\sqrt{2}$. Our BJ model does not satisfy the above conditions unless the staggered structure is assumed.

V. A RANDOM MATRIX APPROACH

We have so far used the two manifold BJ model, where energy correlations are overstated and fluctuations in the coupling are disregarded. Caution must be exercised on the interpretation of what the model indicates. In real molecules, the energy spacings are not equal and the couplings are not constant. It is therefore impossible for every $|\hat{b}\rangle$ dressed state to be paired up with a $|\hat{c}\rangle$ state of the same energy: an eclipsed structure is never reached at any field strength. Most of field dressed states do not overlap in energy with each other. Because of the irregularity of zero-order level energies (e.g., the Wigner distribution), this is the case at any field strength. The features inherent in the staggered structure model will survive to some extent. The point is the ratio between eclipsed structure part and staggered structure part, which is a matter of level statistics. The basic principle is that if the two systems have the same spacing and coupling strength on an average the system with the larger repulsion parameter r has larger $N_{\rm eff}$.

We here propose a random matrix approach that can take into account effects of the energy and coupling distributions on the magnetic quenching, and then consider possible types of distributions at zero field and at the high field limit and the role of spin–vibration interaction. Let the electronic wave function for $|s\rangle$ be $|A\rangle$, and let those for the *b* and *c* manifolds be $|B\rangle$ and $|C\rangle$. The total Hamiltonian can be written as

$$\mathbf{H}=|A\rangle H_A\langle A|+|B\rangle H_B\langle B|+|C\rangle H_C\langle C| +\{|A\rangle V\langle B|+|B\rangle H_Z\langle C|+\text{h.c.}\}, \tag{62}$$

where H_A, H_B, and H_C are the rotation–vibration Hamiltonians for the three electronic states $|A\rangle$, $|B\rangle$, and $|C\rangle$, respectively. We next define the average Hamiltonian and the difference Hamiltonian for H_B and H_C:

$$\bar{H}=(H_B+H_C)/2 \tag{63}$$

and

$$\Delta H_{BC}=H_B-H_C-E_{\rm gap}, \tag{64}$$

where $E_{\rm gap}$ is the zero-field splitting at the equilibrium nuclear configuration of a sublevel potential. Reversibly, H_B and H_C are expressed in terms of $\bar{H}$ and ΔH_{BC}; $H_B=\bar{H}+(E_{\rm gap}+\Delta H_{BC})/2$ and $H_C=\bar{H}-(E_{\rm gap}+\Delta H_{BC})/2$. In Sec. III, we have assumed that the energy gap between the sublevel potentials is a constant $E_{\rm gap}$, irrespective of the nuclear configuration, i.e., $\Delta H_{BC}=0$. In general, the gap depends on the nuclear configuration, i.e., $\Delta H_{BC}\neq 0$. We will present two mechanisms of ΔH_{BC} in Secs. V A and V B.

To write down the matrix elements of $\mathbf{H}$, we introduce the eigenfunctions and eigenvalues of $\bar{H}$:

$$\bar{H}|j\rangle=E_j|j\rangle. \tag{65}$$

The matrix elements of $\mathbf{H}$ for the basis set $\{|j\rangle\}$ are given as

$$\langle j'|\langle B|\mathbf{H}|B\rangle|j\rangle=E_j\delta_{jj'}+\frac{E_{\rm gap}}{2}\,\delta_{jj'}+\frac{\langle j'|\Delta H_{BC}|j\rangle}{2}, \tag{66a}$$

$$\langle j'|\langle C|\mathbf{H}|C\rangle|j\rangle=E_j\delta_{jj'}-\frac{E_{\rm gap}}{2}\,\delta_{jj'}-\frac{\langle j'|\Delta H_{BC}|j\rangle}{2}, \tag{66b}$$

$$\langle s|\mathbf{H}|B\rangle|j\rangle=v_j;\quad \langle j'|\langle B|\mathbf{H}|C\rangle|j\rangle=h_Z\delta_{jj'}. \tag{66c}$$

The parameters $\{E_j, v_j, \langle j'|\Delta H_{BC}|j\rangle\}$ that are inherent in the system are provided by considering a variety of energy distributions and coupling strength distributions. The relation between $N_{\rm eff}/N_0$ and $h_Z/E_{\rm gap}$ is obtained by diagonalizing the matrix at various values of h_Z.

A. The vibrational ΔH_{BC} caused by a combination of spin–spin and vibronic interactions

The spin Hamiltonian generally takes the form

$$H_s=-XS_X^2-YS_Y^2-ZS_Z^2, \tag{67}$$

where S_X, S_Y, and S_Z are the projections of the electron spin operator onto the principal axes. The zero-field splittings caused by spin–spin and spin–orbit interactions, X, Y, and Z

depend on the electronic state.[55,56] For example, each constant of a pure $^3\pi\pi^*$ is different from that of a pure $^3n\pi^*$. These electronic states are vibronically coupled, which leads to the two adiabatic states

$$\Psi_1 = a\Psi_n + b\Psi_\pi; \quad \Psi_2 = a\Psi_\pi - b\Psi_n, \tag{68}$$

where the coefficients a and b are functions of vibronic coupling modes Q and the subscripts π and n refer to the pure $^3\pi\pi^*$ and $^3n\pi^*$ states. The zero-field splittings for these adiabatic states are functions of nuclear coordinates, for instance,[55]

$$X_1(Q) = |a|^2 X_n + |b|^2 X_\pi + ; \quad Y_1(Q) = |a|^2 Y_n + |b|^2 Y_\pi + . \tag{69}$$

If only two spin sublevels in the state Ψ_1 are considered, ΔH_{BC} can be written as

$$\begin{aligned}\Delta H_{BC} &= [X_1(Q) - Y_1(Q)] - [X_1(0) - Y_1(0)] \\ &= (a^2 - 1)(X_n - Y_n) + b^2(X_\pi - Y_\pi) + \cdots . \end{aligned} \tag{70}$$

As the nuclear configuration is shifted from the equilibrium one, the value of ΔH_{BC} can change a few times as much as $E_{\rm gap}$. In this mechanism (the vibrational ΔH_{BC}), ΔH_{BC} is a function of vibrational degrees of freedom. The role of ΔH_{BC} is examined for the following three cases.

1. Case M: Nonintegrable, strongly coupled systems with $\Delta H_{BC}=0$

Consider the $\bar{H}$ that has f vibrational degrees of freedom. If the corresponding modes are strongly coupled, or at high vibrational energies, the level spacing distribution fits the Wigner distribution well. First, we generate energy spacings from a Wigner distribution. The average spacing is denoted by ε. The energies of levels are then located in the energy axis by piling up those spacings (in this sense higher order level correlations that the GOE should possess are not taken into account but they do not play the key role in the present context). We choose the coupling strengths v_j from a Gaussian distribution[44,57] with dispersion of $(4.5\varepsilon)^2$ and set $E_{\rm gap}=100\varepsilon$. Another condition imposed is that $\Delta H_{BC}=0$ (this restriction will be released in case H). Figure 15(a) shows the field dependence of $N_{\rm eff}/N_0$ ($N_0 \approx 120$). Seven sets of random numbers are generated for preparing Wigner distributions that have the same average spacing ε and Gaussian distributions that have the same coupling dispersion $(4.5\varepsilon)^2$. The different marks in Fig. 15(a) correspond to different sets. Almost all values of $N_{\rm eff}/N_0$ are smaller than the values (solid line) given by Eq. (60). Even at $h_Z/E_{\rm gap}=2$, the average value of $N_{\rm eff}/N_0$ is much smaller than the value of 2 that is expected from the increase in the background level density. This is explained by the level clustering of dressed states that are coupled to $|s\rangle$. At zero field, the spacing distribution is a Brody distribution with $r=1$, i.e., a Wigner distribution. On the other hand, at the high field limit, the spacing distribution of dressed states is a combined distribution of two Wigner distributions mutually shifted by $E_{\rm gap}$. This distribution is well approximated by a Brody distribution with $r \approx 0.36$ (and the average spacing $D=\varepsilon/2$). As h_Z is increased, the ratio of overlapping levels becomes higher: the value $N_{\rm eff}/N_0$ does not increase as rapid as Eq. (60) and never reaches 2 on an average.

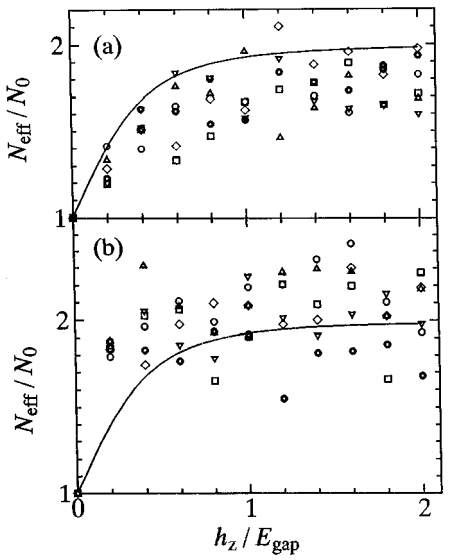

FIG. 15. Relations between $N_{\rm eff}/N_0$ and $h_Z/E_{\rm gap}$ in the random matrix model. The energies of levels are determined by piling up those spacings that are generated from a Wigner distribution of average spacing ε. The coupling strengths v_j are generated from a Gaussian distribution with dispersion of $(4.5\varepsilon)^2$ ($E_{\rm gap}=100\varepsilon$). Seven sets of random numbers are generated for preparing Wigner distributions that have the same average spacing ε and Gaussian distributions that have the same coupling dispersion $(4.5\varepsilon)^2$. The different marks in the figure correspond to different sets. (a) $\Delta H_{BC}=0$ and (b) $\overline{|\langle j|\Delta H_{BC}|j'\rangle|^2}=(2\varepsilon)^2$.

2. Case L: Integrable, weakly coupled systems

If f degrees of freedom are independent or only weakly coupled (at low vibrational energies), the eigenstate is defined by f quantum numbers. Those eigenfunctions of roughly the same energy typically look very different (they have completely different nodal patterns). Where these functions overlap in configuration space, they beat violently against each other: the matrix elements $\langle j|\Delta H_{BC}|j'\rangle$ of the smooth potential ΔH_{BC} are very small, compared to the average level spacing. ΔH_{BC} couples strongly only states that do not differ greatly from each other in the assignment of vibrational quantum numbers; these states are separated at least by energy of one quantum. Therefore we expect $\langle j|\Delta H_{BC}|j'\rangle$ to be effectively zero.

At zero field, the spacing distribution will be a Poisson distribution. At the high field limit, the spacing distribution is a combined distribution of two Poisson distributions mutually shifted by $E_{\rm gap}$ (no interactions between them), which remains to be a Poisson distribution. That is, the distribution becomes a Poisson with $D=\varepsilon/2$ and the average coupling strength is reduced to $(\overline{v_j^2})^{1/2}/\sqrt{2}$. If the couplings were constant, $N_{\rm eff}/N_0$ would approach 2 as h_Z increases. For this case, we have numerically confirmed that $N_{\rm eff}/N_0$ increases nearly as rapid as Eq. (60).

However, for the integrable system, where selection rules operate, some couplings are expected to be strong and many others will be very weak. Clustering levels of a Pois-

son distribution will have coupling strengths of different orders of magnitude. Consider two nearly degenerate levels. Since they have completely different nodal patterns (otherwise they would repel each other), one of the levels will be strongly coupled to $|s\rangle$ and the other level is not. The levels that are weakly coupled to $|s\rangle$ can be combed out of the background levels $\{|j\rangle\}$. The combed background manifold looks as if level clustering is removed to some extent (level clustering is substantially less effective in the combed background manifold than in the Poisson distribution with constant coupling). In the level structure at the high field limit, obtained by superimposing the combed background manifold on the same one shifted by $E_{\rm gap}$ (note that $\langle j|\Delta H_{BC}|j'\rangle=0$), many levels with relatively large coupling strengths cluster. The degree of level clustering is larger at high fields than at low fields. As h_Z is increased, the ratio of overlapping levels becomes higher and $N_{\rm eff}/N_0$ increases more slowly than Eq. (60). The maximum value of $N_{\rm eff}/N_0$ is less than 2 (on an average), as in Fig. 15(a). These features, which are also observed in case M, explain why magnetic quenching is inefficient for molecules of small energy separation between S_1 and T_1 (except excitation onto high rotational levels).

3. Case H: Nonintegrable, strongly coupled systems with relatively large $\Delta H_{BC}\neq 0$

The ΔH_{BC}, which is as small as $E_{\rm gap}$, do not affect the energies and coupling strengths for low vibrational levels which are mutually separated at spacings much larger than ΔH_{BC}. However, the case is different for strongly coupled systems at high energies, i.e., for chaotic systems of which average spacings are less than, say, 0.01 $\rm cm^{-1}$. For the ''irregular'' regime of phase space where the classical motion is ergodic,[58] the following assumptions that no integrable systems meet are justified semiclassically:[59] (i) each eigenfunction is spread over the entire classically allowed region of configuration space appropriate to its energy; (ii) its coarse-grained probability density in phase space agrees well with the classical microcanonical density at that energy; (iii) the ergodic wave functions should be ''Gaussian random'' functions of the coordinates $\mathbf{q}$, i.e., $\langle\mathbf{q}|j\rangle$ be Gaussian random (a Gaussian random $\langle\mathbf{q}|j\rangle$ leads to a Gaussian random v_j).[44] Heller *et al.*[60] have found that an eigenstate in the irregular regime can display a networked narrow ridge (called ''scars'') with enhanced intensities which stands out clearly and appears to be coming from classical periodic orbits. It is obvious that periodic orbit scar localization contradicts assumptions (i) and (ii). Since the ratio of those states to states that satisfy conditions (i), (ii), and (iii) will decrease to measure zero with increasing energy, we do not count eigenstates of scar localization, i.e., we use all three assumptions in the following qualitative discussion.

If the three features are accepted, there are no strong selection rules for $\langle j|\Delta H_{BC}|j'\rangle$. For wave functions of roughly the same energy, these matrix elements are of the same order of magnitude. Since $\langle\mathbf{q}|j\rangle$ are Gaussian random functions of the coordinates, the matrix elements $\langle j|\Delta H_{BC}|j'\rangle$ $(=\int d\mathbf{q}\int d\mathbf{q}'\langle j|\mathbf{q}\rangle\langle\mathbf{q}|\Delta H_{BC}|\mathbf{q}'\rangle\langle\mathbf{q}'|j'\rangle)$ of the smooth potential ΔH_{BC} would be a Gaussian random with respect to states $|j\rangle$ and $|j'\rangle$. Let us estimate the order of magnitude of the dispersion $\overline{|\langle j|\Delta H_{BC}|j'\rangle|^2}$. A given state $|j\rangle$ couples mainly to states that lie within a range ΔE_c around E_j. Outside the range, the mismatch in local wavelength kills the integral $\langle j|\Delta H_{BC}|j'\rangle$. ΔE_c is defined such that $\langle j|\Delta H_{BC}|j'\rangle=0$ if $|E_j-E_{j'}|>\Delta E_c$. From the sum rule[61]

$$\sum_{j'}|\langle j|\Delta H_{BC}|j'\rangle|^2=\langle j|\Delta H_{BC}^2|j\rangle=O(\Delta H_{BC}^2) \tag{71}$$

the dispersion $\overline{|\langle j|\Delta H_{BC}|j'\rangle|^2}$ is estimated to be $O(\Delta H_{BC}^2)(\varepsilon/\Delta E_c)$. Upon letting $\Delta E_c=50$ $\rm cm^{-1}$ and $\varepsilon=10^{-3}$ $\rm cm^{-1}$, the rms of $\langle j|\Delta H_{BC}|j'\rangle$ becomes as large as the average level spacing.

Figure 15(b) is the result for $\overline{|\langle j|\Delta H_{BC}|j'\rangle|^2}=(2\varepsilon)^2$ [the other parameters are the same as in Fig. 15(a)]. Smoothing the fluctuation, one finds that the calculated $N_{\rm eff}/N_0$ grows as rapid as or more rapidly than Eq. (60). This suggests that the background dressed states obtained by diagonalization of $\mathbf{H}$-V form a staggered structure owing to nonzero elements of $\langle j|\Delta H_{BC}|j'\rangle$ (the background dressed state structure can be revealed by setting $v_j=0$). We have confirmed that around $h_Z/E_{\rm gap}=2$ the background dressed states form a spacing distribution represented by a Brody distribution of $r=0.95$ (the average level spacing is $\varepsilon/2$) and their couplings to $|s\rangle$ form a Gaussian random distribution of dispersion $(4.5\varepsilon)^2/2$. For pyrazine, the S_1-T_1 separation is $\sim$4500 $\rm cm^{-1}$ and the S_1-T_2 separation is $\sim$2900 $\rm cm^{-1}$. At the S_1 origin, the vibrational density of states in the triplets is $2-5\times10^{-3}$ $\rm cm^{-1}$:[25] vibrational modes in the triplets are expected to be rather strongly coupled. The efficient magnetic quenching in pyrazine is explained by the formation of staggered structure due to the vibrational ΔH_{BC}.

The mechanism that a staggered structure is formed at high fields is explained as follows. Because of nonzero elements of $\langle j|\Delta H_{BC}|j'\rangle$, isoenergetic levels belonging to different spin sublevels ($|b_j\rangle$ and $|c_{j'}\rangle$) have small but nonzero vibrational overlap. Then, the magnetic field opens up direct paths between them (which is another factor to enhance the efficiency of magnetic quenching). The interaction energy between the corresponding dressed states $|\hat{b}_j\rangle\}$ and $\{|\hat{c}_{j'}\rangle$ is estimated to be

$$\langle\hat{b}_j|\mathbf{H}|\hat{c}_{j'}\rangle=-\sin 2\theta\langle j|\frac{\Delta H_{BC}}{2}|j'\rangle. \tag{72}$$

If the interaction energy is as large as the average spacing ε, level repulsion occurs in a wide range of energy. The wide-ranging level repulsion causes a staggered structure accompanied by isoenergetic intermanifold mixing. For this magnitude of $\langle j|\Delta H_{BC}|j'\rangle$, $|j\rangle$ is distributed among $\{|b_j\rangle\}$ or $\{|c_j\rangle\}$ over a width of about 10ε which is much less than $E_{\rm gap}$: the meaning of the energy gap $E_{\rm gap}$ is not fully lost.

B. The rotational ΔH_{BC} caused by a combination of spin–rotation and rotation–vibration interactions

Because of the interaction of unpaired electron spins with the magnetic fields created by molecular rotation (spin–rotation interaction),[62] the zero-field splittings depend on the rotational state. For simplicity, we use the oblate symmetric

top approximation and define the rotational state by the quantum numbers N,K. The spin–rotation interaction can then be included in the H_A and H_B as follows:

$$H_B = H_v + H_{rv} + \sum_{N,K} F_B(N,K)|N,K\rangle\langle N,K|, \tag{73}$$

$$H_C = H_v + H_{rv} + \sum_{N,K} F_C(N,K)|N,K\rangle\langle N,K|, \tag{74}$$

where H_v represents the vibrational Hamiltonian, H_{vr} the rotation–vibration interaction (Coriolis interaction), $F_B(N,K)$ and $F_C(N,K)$ the rotational energies for the spin sublevels associated with $|N,K\rangle$. $F_B(N,K)$ and $F_C(N,K)$ include the spin–spin, spin–orbit, and spin–rotation interactions. Let $F_B(N,K)$ and $F_C(N,K)$ correspond to the rotational terms $F_2(N,K)$ and $F_1(N,K)$, respectively. They have been derived by Raynes[63,64]

$$F_2(N,K) = E_r(N,K) + \frac{3K^2(a-\alpha)}{N(N+1)}, \tag{75}$$

$$F_1(N,K) = E_r(N,K) - \frac{3(N+1)\alpha}{2N+3} + (a-a_0)(N+1) - \frac{3K^2}{N+1}\left(a - \frac{\alpha}{2N+3}\right), \tag{76}$$

where $E_r(N,K)$ is the purely rotational energy, the constants a_0 and a originate from the spin–rotation interaction, and α originates from the spin–spin interaction.[62] These constants also include effects of spin–orbit interaction. (The meanings of these constants are the same as those in Ref. 63.) In the following, we replace $F_B(N,K)$ and $F_C(N,K)$ with $F_2(N,K)$ and $F_1(N,K)$ whenever it is necessary.

For the above set of Hamiltonians, the difference Hamiltonian ΔH_{BC} is

$$\Delta H_{BC} = \sum_{N,K} \Delta F_{BC}(N,K)|N,K\rangle\langle N,K|, \tag{77}$$

where

$$\Delta F_{BC}(N,K) = [F_B(N,K) - F_C(N,K)] - [F_B(0,0) - F_C(0,0)]. \tag{78}$$

This rotational ΔH_{BC}, which is a function of rotational degrees of freedom, never mixes $\{|j\rangle\}$ if the rotation–vibration interactions are weak, i.e., when the total wave function can be well approximated as a single product of $|N,K\rangle$ and the vibrational wave function $|\phi_v\rangle$ (of which energy is E_v, i.e., $H_v|\phi_v\rangle = E_v|\phi_v\rangle$). However, the rotational ΔH_{BC} mixes $\{|j\rangle\}$ if a- and b-axis Coriolis couplings cause K mixing to a great extent. Consider two states $|\phi_v\rangle|N,K\rangle$ and $|\phi_{v'}\rangle|N,K'\rangle$ that are mixed by the Coriolis interactions as

$$|j\rangle = \cos\,\xi|\phi_v\rangle|N,K\rangle + \sin\,\xi|\phi_{v'}\rangle|N,K'\rangle, \tag{79}$$

$$|j'\rangle = \cos\,\xi|\phi_{v'}\rangle|N,K'\rangle - \sin\,\xi|\phi_v\rangle|N,K\rangle, \tag{80}$$

where

$$\xi = \frac{1}{2}\tan^{-1}\frac{2\langle N,K|\langle\phi_v|H_{rv}|\phi_{v'}\rangle|N,K\rangle}{E_v + [F_B(N,K)+F_C(N,K)]/2 - E_{v'} - [F_B(N,K')+F_C(N,K')]/2}. \tag{81}$$

For this case, ΔH_{BC} mixes the functions $|j\rangle$ and $|j'\rangle$ which are considered eigenfunctions of the average Hamiltonian $\bar{H}$:

$$\langle j|\Delta H_{BC}|j'\rangle = \frac{\sin 2\xi}{2}[\Delta F_{BC}(N,K') - \Delta F_{BC}(N,K)] = \frac{\sin 2\xi}{2}\frac{3(K+K')(K'-K)}{N}\left(a - \frac{3\alpha}{2N+3}\right). \tag{82}$$

It is not so difficult to treat cases where many states are mixed by rotation–vibration interaction. In general, $|j\rangle$ takes the form

$$|j\rangle = \sum_K |\phi_{j,K}\rangle|N,K\rangle, \tag{83}$$

where $|\phi_{j,K}\rangle$ contains only the vibrational degrees of freedom. Using the sum rule [see Eq. (71)], we find that

$$\sum_{j'} |\langle j|\Delta H_{BC}|j'\rangle|^2 = \sum_K |\langle\phi_{j,K}|\phi_{j,K}\rangle|^2 \Delta F_{BC}^2(N,K) \approx \frac{1}{2N+1}\sum_K \Delta F_{BC}^2(N,K) = \frac{18(N+1)(3N^2+3N-1)}{30N}\left(a - \frac{3\alpha}{2N+3}\right) + N^2\left(a_0 - a + \frac{\alpha}{2N+3}\right)^2 + 2N(N+1)\left(a_0 - a + \frac{\alpha}{2N+3}\right) \approx (a_0^2 + a^2)N^2, \tag{84}$$

where all the K components are assumed to be equally populated in $|j\rangle$ owing to a- and b-axis Coriolis couplings. Nonzero matrix elements of $\langle j|\Delta H_{BC}|j'\rangle$ will be distributed among $(2N+1)N_P$ levels that are energetically near $|j\rangle$, where N_P is the number of vibrational levels mixed by the Coriolis couplings[52,53] (N_P is regarded as the number of nearly degenerate vibrational levels belonging to the same polyad).[65] The dispersion is thus expected to be

$$\overline{|\langle j|\Delta H_{BC}|j'\rangle|^2} = \frac{(a_0^2+a^2)N^2}{(2N+1)N_P}. \tag{85}$$

The condition that a staggered structure is formed is that the rms of $\langle j|\Delta H_{BC}|j'\rangle$ is larger than the average level spacing including the rotational degrees of freedom,

$$\sqrt{\frac{(a_0^2+a^2)N^2}{(2N+1)N_P}} \geqslant \frac{\varepsilon}{2N+1}, \tag{86}$$

where ε is the average spacing for $N=0$ (the purely vibrational spacing).

Take *s*-triazine, for example.[23,66] This molecule is kind of a small molecule, since the triplet density of vibrational states ε is $\sim 1\ \mathrm{cm}^{-1}$ at the 6^1 vibrational level of S_1: the magnetic quenching at this band is inefficient for low $J' \leqslant 5$ (under collision-free conditions, the amount of quenching at 150 G is 10% of the fluorescence quantum yield at zero field). Since the energy separation between the 6^1 of S_1 and the T_1 origin is only about $1700\ \mathrm{cm}^{-1}$, the vibrational ΔH_{BC} does not induce a staggered structure. However, in the bulk gas at 250 mTorr, where the average J' is about 30, the amount of quenching at 150 G reaches 40% of the fluorescence quantum yield at zero field. We attribute this to the formation of a staggered structure due to the rotational ΔH_{BC}. The typical values of a_0 and a for intermediate case molecules are expected to be about $0.01\ \mathrm{cm}^{-1}$ ($0.02\ \mathrm{cm}^{-1}$ for the lowest triplet of H_2CO of which rotational constants are larger than those of *s*-triazine).[63] Considering anharmonic constants, N_P would be less than 50. The inequality (86) is fulfilled for the set of these values ($N \sim J' = 30$).

VI. SUMMARY AND CONCLUSIONS

In this paper, the effect of magnetic field on ISC has been modeled by including two background manifolds $\{|b_j\rangle\}$ and $\{|c_j\rangle\}$ mutually shifted by the zero-field splitting E_{gap}; the $\{|b_j\rangle\}$ manifold is coupled to the singlet bright level $|s\rangle$ by the intramolecular interaction V and the two manifolds are coupled by the Zeeman interaction H_Z. The two manifold model features the magnetic field effect on ISC, though a triplet electronic state has three spin sublevels. The model is analyzed on the basis of the two manifold BJ model and the random matrix approach. In the two manifold BJ model, it has been assumed that the background level spacings and the couplings to $|s\rangle$ are constant (ε and v) and no spin–vibration interactions exist (the Zeeman interaction connects only the spin sublevels of the same rovibronic level j and does not connect the spin sublevels of different rovibronic levels). In the random matrix approach that can take into account level statistics, the role of indirect spin–vibration interactions in magnetic quenching has been examined.

By analyzing the two manifold BJ model, we have found that two extreme energy structures, namely, the eclipsed and staggered structures, are of special importance. They are defined by using the field dressed states for the background Hamiltonian $H_0+H_Z(=\mathbf{H}-V)$. There are two sets of field dressed states, $\{|\hat{b}_j\rangle\}$ and $\{|\hat{c}_j\rangle\}$ ($|\hat{b}_j\rangle$ and $|\hat{c}_j\rangle$ are liner combinations of $|b_j\rangle$ and $|c_j\rangle$). We call the structure eclipsed when the two sets of dressed states overlap in energy and call it staggered when every $|\hat{b}\rangle$ state is just between two adjacent $|\hat{c}\rangle$ states. The energies of the field dressed states shift with the Zeeman energy h_Z. The eclipsed and staggered structures alternatively appear at intervals of about $\varepsilon/2$ in h_Z.

Between the two cases there is a major difference; with increasing h_Z the number of effectively coupled background levels, N_{eff}, increases for the staggered structure but remains unchanged for the eclipsed structure. When two dressed states are degenerate (in the eclipsed case, every $|\hat{b}\rangle$ dressed state energetically coincides with one of $|\hat{c}\rangle$ states), it is always possible, irrespective of their coupling strengths, to find a transformation under which one state carries coupling strength to $|s\rangle$ and the other does not. This is the reason why N_{eff} remains constant with increasing h_Z if the level structure is restricted to the eclipsed one.

What the staggered structure model suggests is in accord with experimental results on the magnetic quenching. In the far wing regions of the absorption band, the field dressed states $\{|\hat{b}_j\rangle\}$ and $\{|\hat{c}_j\rangle\}$ are approximate eigenstates of the total Hamiltonian **H**. In these regions, an eigenstate contains only one *b*-character level and only one *c*-character level (a pair of levels connected by the Zeeman interaction) and the mixing between the two levels $|b_j\rangle$ and $|c_j\rangle$ is determined by the ratio h_Z/E_{gap}: the mixing between zero-order levels (intermanifold mixing) is small as long as the ratio h_Z/E_{gap} is small. On the other hand, near the absorption band center, the *s* component is transferred to background levels $\{|c_j\rangle\}$ by the second-order Raman-like process due to V and H_Z, which distributes the *s* character to more eigenstates (intermanifold mixing isoenergetic to $|s\rangle$). The intermanifold mixing is enhanced by the presence of the doorway $|s\rangle$ level (or V). Consequently, if the levels structure is restricted to the staggered one, N_{eff} increases with increasing h_Z more rapidly than expected for the far wing regions.

In the two manifold BJ model, energy correlations are overstated and fluctuations in the coupling are disregarded. In real molecules, the energy spacings are not equal and the couplings are not constant. It is impossible for every $|\hat{b}\rangle$ dressed state to be paired with a $|\hat{c}\rangle$ state of the same energy. As long as spin and vibration do not interact with each other it is also impossible for all the dressed states to be nondegenerate. Neither perfect eclipsed structure nor perfect staggered structure are possible. The problem is that if a perfect staggered structure is impossible even very high fields will not reduce the quantum yield to 1/2 (for $M=2$) of the zero-field value contrary to the experimental fact.

Necessary conditions for the complete magnetic quenching (that the quantum yield is reduced to 1/2 at high fields) are: (i) the energy distribution of dressed states at high fields is the same type as that of the *b* manifold and the average spacing is reduced to $\varepsilon/2$; (ii) the coupling distribution at high fields is the same type of that of the *b* manifold and the rms of the coupling is reduced to $(\overline{v_j^2})^{1/2}/\sqrt{2}$. Our BJ model does not satisfy the above conditions unless the staggered structure is assumed. We have solved the problem by using the random matrix approach that can consider level statistics of background levels and spin–vibration interaction.

In the random matrix approach, the doorway electronic state $|A\rangle$ and two background electronic states $|B\rangle$ and $|C\rangle$ are introduced. The total Hamiltonian **H** is constructed of the

rotation–vibration Hamiltonians for the three electronic states involved, H_A, H_B, and H_C. The difference $\Delta H_{BC} \equiv H_B - H_C - E_{\rm gap}$ plays the key role, where $E_{\rm gap}$ is the zero-field splitting at the equilibrium nuclear configuration. In the presence of spin–vibration interaction, the energy gap between the sublevel potentials depends on the nuclear configuration, i.e., $\Delta H_{BC} \neq 0$. Two mechanisms of ΔH_{BC} have been presented: the ΔH_{BC} caused by a combination of spin–spin and vibronic interactions (the vibrational ΔH_{BC}) and the ΔH_{BC} caused by a combination of spin–rotation and rotation–vibration interactions (the rotational ΔH_{BC}).

The vibrational ΔH_{BC} is a function of vibrational degrees of freedom and the rotational ΔH_{BC} is a function of rotational degrees of freedom. The matrix elements of **H** are written down in terms of the eigenfunctions $\{|j\rangle\}$ and eigenvalues $\{E_j\}$ of the average Hamiltonian $(H_B + H_C)/2$. The role of the vibrational ΔH_{BC} depends on the density of vibrational states and on how strongly the vibrational modes are coupled.

For a system where the vibrational modes are strongly coupled, the energies of levels are given by a Wigner distribution and the coupling strengths are given by a Gaussian distribution. If the rms of $\langle j|\Delta H_{BC}|j'\rangle$ is smaller than the average level spacing, the calculated values of $N_{\rm eff}/N_0$ are, on an average, smaller than Eq. (60) for the staggered case in the two manifold BJ model. At zero field, the spacing distribution is a Brody distribution with the repulsion parameter $r=1$, i.e., a Wigner distribution, but at the high field limit, the spacing distribution of dressed states is a combined distribution of two Wigner distributions mutually shifted by $E_{\rm gap}$. This distribution is well approximated by a Brody distribution with $r \approx 0.36$. As h_Z is increased, the ratio of overlapping levels becomes higher: the value $N_{\rm eff}/N_0$ does not increase as rapidly as Eq. (60) and never reaches 2 on an average.

For weakly coupled systems, the spacing distribution will be a Poisson distribution. The eigenfunctions of roughly the same energy typically look very different and they beat violently against each other: the matrix elements $\langle j|\Delta H_{BC}|j'\rangle$ are negligible. Consequently, the spacing distribution at the high field limit is a combined distribution of two Poisson distributions mutually shifted by $E_{\rm gap}$, which remains to be a Poisson distribution (the average spacing and coupling strength are, respectively, reduced to 1/2 and to $1/\sqrt{2}$). If the couplings were constant, with increasing h_Z, $N_{\rm eff}/N_0$ would approach 2 and $N_{\rm eff}/N_0$ increases nearly as rapid as Eq. (60). However, for weakly coupled systems, where selection rules operate, some couplings are expected to be strong and many others will be very weak. Clustering levels of a Poisson distribution will have coupling strengths of different orders of magnitude. The levels that are weakly coupled to $|s\rangle$ can be combed out of the background levels $\{|j\rangle\}$. The combed background manifold looks as if level clustering is removed to some extent. In the level structure at the high field limit, obtained by superimposing the combed background manifold on the same one shifted by $E_{\rm gap}$, many levels with relatively large coupling strengths cluster. The degree of level clustering is larger at high fields than at low fields. As h_Z is increased, the ratio of overlapping levels becomes higher and $N_{\rm eff}/N_0$ increases more slowly than Eq. (60). The maximum value of $N_{\rm eff}/N_0$ is less than 2 (on an average). These features explain why magnetic quenching is inefficient in molecules of small energy separation between S_1 and T_1.

For strongly coupled systems, there are no strong selection rules for $\langle j|\Delta H_{BC}|j'\rangle$. For wave functions of roughly the same energy, these matrix elements are Gaussian random. The dispersion $\overline{|\langle j|\Delta H_{BC}|j'\rangle|^2}$ is estimated to be $O(\Delta H_{BC}^2)(\bar{\in}/\Delta E_c)$, where ΔE_c is the range outside which the mismatch in local wavelength between wave functions kills the integral $\langle j|\Delta H_{BC}|j'\rangle$. Upon letting $\Delta E_c = 50\ {\rm cm}^{-1}$ and $\varepsilon = 10^{-3}\ {\rm cm}^{-1}$, the rms of $\langle j|\Delta H_{BC}|j'\rangle$ becomes as large as the average level spacing. When the rms of $\langle j|\Delta H_{BC}|j'\rangle$ is as large as the average spacing, the calculated $N_{\rm eff}/N_0$ grows as rapidly as Eq. (60). Nonzero elements of $\langle j|\Delta H_{BC}|j'\rangle$ let isoenergetic levels belonging to different spin sublevels ($|b_j\rangle$ and $|c_{j'}\rangle$) vibrationally overlap. The effect of ΔH_{BC} is therefore twofold: the ΔH_{BC}, together with the magnetic field causes wide-ranging level repulsion leading to a staggered structure (which is accompanied by the efficient isoenergetic intermanifold mixing) and opens up isoenergetic paths between the two manifolds (which also enhance the efficiency of magnetic quenching). The efficient magnetic quenching in pyrazine can be explained by the formation of staggered structure due to the vibrational ΔH_{BC}, since the $S_1 - T_1$ separation is as large as 4500 $\rm cm^{-1}$.

The rotational ΔH_{BC} mixes $\{|j\rangle\}$ if a- and b-axis Coriolis (in the oblate case) couplings cause K mixing considerably. Nonzero matrix elements of $\langle j|\Delta H_{BC}|j'\rangle$ will be distributed among $(2N+1)N_P$ levels that are energetically near $|j\rangle$, where N_P is the number of vibrational levels mixed by the Coriolis couplings. Then, the condition that a staggered structure is formed is Eq. (86), i.e., the inequality that the rms of $\langle j|\Delta H_{BC}|j'\rangle$ is larger than the average level spacing including the rotational degrees of freedom. It is known for s-triazine that for low $J' \leqslant 5$ the amount of quenching at 150 G is 10% of the fluorescence quantum yield at zero field but in the bulk gas (the average $J' \sim 30$) it amounts to 40%. We attribute this to the formation of a staggered structure due to the rotational ΔH_{BC}, since the energy separation between the S_1 and T_1 origins is only about 1000 $\rm cm^{-1}$.

The question left to us is a quantitative one: How much do the characteristic mechanisms proposed in this paper function in real molecules? We should employ methods of discussing quantitatively without providing energy levels and their couplings *a priori*. That is, potential surfaces are input data. In a previous paper,[67] we have presented a method (the filtered energy Lanczos method) to simulate intermediate case radiationless transitions for given potentials. The strategy consists of three steps: (1) computation of an optically prepared state at a time just after the pump pulse has decayed; (2) extraction of eigenfunctions from the optically prepared state; (3) calculation of time-dependent quantities such as the fluorescence intensity using the eigenfunctions obtained. The first step can be carried out by time-dependent methods for wave-packet dynamics.[68,69] In the second step, Lanczos vectors are generated, from the prepared state, with an energy filtered Hamiltonian and diagonalize the unfiltered

Hamiltonian. Preliminary calculations have been performed for systems of two vibrational degrees of freedom (the density of states is $\sim 20/\mathrm{cm}^{-1}$): an accuracy of 10^{-5} cm^{-1} can easily be obtained. The long time dynamics up to ~ 1 μs is within reach. As shown in this paper, magnetic quenching can be discussed by calculating N_{eff} from the eigenfunctions (also by calculating the time-resolved fluorescence signal). Correlation between energy and coupling will be adequately taken into account by putting realistic potential surfaces. Work based on these approaches will be reported elsewhere.

To conclude this paper we would like to point out that the problem we are tackling is not restricted to the magnetic quenching of fluorescence but rather general: What happens when three or more sequentially coupled potential surfaces are involved in the dynamics? Our model implies that energy transfer or mixing is enhanced by adding more potential surfaces.

ACKNOWLEDGMENTS

This work was supported in part by Grant-in-Aid for Scientific Research from the Ministry of Education, Science and Culture, Japan, Grant No. 06218204 on Priority Area ''Molecular Magnetism'' (Area No. 228). We thank Dr. H. Hayashi and Dr. H. Abe for most helpful interactions. One of the authors (H.K.) acknowledges Dr. S. Yamauchi for helpful discussions.

[1] J. Jortner, S. A. Rice, and R. M. Hochstrasser, Adv. Photochem. **7**, 149 (1969).
[2] J. Jortner and R. D. Levine, in *Photoselective Chemistry, Advances in Chemical Physics*, edited by J. Jortner, R. D. Levine, and S. A. Rice (Wiley, New York, 1981), Vol. 47, p. 1.
[3] G. W. Robinson, in *Excited States*, edited by E. C. Lim (Academic, New York, 1974), Vol. 1, p. 1.
[4] A. Tramer and R. Voltz, in *Excited States*, edited by E. C. Lim (Academic, New York, 1979), Vol. 4, p. 281.
[5] *Radiationless Transitions*, edited by S. H. Lin (Academic, New York, 1980).
[6] J. Kommandeur, W. A. Majewski, W. L. Meerts, and D. W. Pratt, Annu. Rev. Phys. Chem. **38**, 433 (1987); J. Kommandeur, Adv. Chem. Phys. **70**, 133 (1988); K. E. Drabe and J. Kommandeur, in *Excited States*, edited by E. C. Lim (Academic, New York, 1988), Vol. 7, p. 107.
[7] M. Bixon and J. Jortner, J. Chem. Phys. **48**, 715 (1968).
[8] C. G. Stevens and J. C. D. Brand, J. Chem. Phys. **58**, 3324 (1973).
[9] G. Herzberg, *Electronic Spectra and Electronic Structure of Polyatomic Molecules* (Van Nostrand, Princeton, 1966).
[10] M. Lombardi, R. Jost, C. Michel, and A. Tramer, Chem. Phys. **57**, 341 (1981); M. Lombardi, in *Excited States*, edited by E. C. Lim (Academic, New York, 1988), Vol. 7, p. 163.
[11] W. E. Howard and E. W. Schlag, in Ref. 5, p. 81.
[12] J. C. D. Brand, C. di Lauro, and D. S. Liu, Can. J. Phys. **53**, 1853 (1975).
[13] P. R. Stannard, J. Chem. Phys. **68**, 3932 (1978); A. Matsuzaki and S. Nagakura, Helv. Chim. Acta **61**, 675 (1978).
[14] S. H. Lin and Y. Fujimura, in *Excited States*, edited by E. C. Lim (Academic, New York, 1979), Vol. 4, p. 237.
[15] U. E. Steiner and T. Ulrich, Chem. Rev. **89**, 51 (1989).
[16] P. M. Felker, Wm. R. Lambert, and A. H. Zewail, Chem. Phys. Lett. **89**, 309 (1982).
[17] D. M. Burland and J. Schmidt, Mol. Phys. **22**, 19 (1971).
[18] Y. Matsumoto, L. H. Spangler, and D. W. Pratt, J. Chem. Phys. **80**, 5539 (1984).
[19] Y. Matsumoto, L. H. Spangler, and D. W. Pratt, Chem. Phys. Lett. **98**, 333 (1983); Laser Chem. **2**, 91 (1983).
[20] N. Ohta and T. Takemura, J. Chem. Phys. **91**, 4477 (1989).
[21] N. Ohta and T. Takemura, J. Chem. Phys. **95**, 7119 (1991).
[22] N. Ohta and T. Takemura, J. Chem. Phys. **95**, 7133 (1991).
[23] N. Ohta and T. Takemura, Trends Chem. Phys. **1**, 447 (1991).
[24] N. Ohta and T. Takemura, Chem. Phys. **162**, 15 (1992).
[25] D. B. McDonald, G. R. Fleming, and S. A. Rice, Chem. Phys. **60**, 335 (1981).
[26] H. Abe and H. Hayashi, Chem. Phys. Lett. **206**, 337 (1993).
[27] A. Amirav and J. Jortner, J. Chem. Phys. **84**, 1500 (1986).
[28] A. Amirav, Chem. Phys. **126**, 327 (1988); A. Amirav and Y. Oreg, *ibid*. **126**, 343 (1988); A. Amirav, *ibid*. **126**, 365 (1988).
[29] H. Saigusa and E. C. Lim, Chem. Phys. Lett. **88**, 455 (1982); J. Chem. Phys. **78**, 91 (1983).
[30] H. Baba, M. Fujita, and K. Uchida, Chem. Phys. Lett. **73**, 425 (1980); H. Baba, N. Ohta, O. Sekiguch, M. Fujita, and K. Uchida, J. Phys. Chem. **87**, 943 (1983); O. Sekiguchi, N. Ohta, and H. Baba, Chem. Phys. Lett. **106**, 387 (1984).
[31] T. A. Brody, J. Flores, J. B. French, P. A. Mello, A. Pandey, and S. S. M. Wong, Rev. Mod. Phys. **53**, 385 (1981); O. Bohigas and M. J. Giannoni, Lecture Notes Phys. **209**, 1 (1984); M. L. Mehta, *Random Matrices* (Academic, New York, 1991).
[32] W. Rhodes, in Ref. 5, p. 219.
[33] H. Kono, Y. Fujimura, and S. H. Lin, J. Chem. Phys. **75**, 2569 (1981).
[34] A. Frad, F. Lahmani, A. Tramer, and C. Tric, J. Chem. Phys. **60**, 4419 (1974); F. Lahmani, A. Tramer, and C. Tric, *ibid*. **60**, 4431 (1974).
[35] J. M. Delory and C. Tric, Chem. Phys. **3**, 54 (1974).
[36] M. V. Berry and M. Tabor, Proc. R. Soc. London Ser. A **356**, 375 (1977).
[37] H. Bitto, S. Derler, and J. R. Huber, Chem. Phys. Lett. **162**, 291 (1989).
[38] L. Leviandier, M. Lombardi, R. Jost, and J. P. Pique, Phys. Rev. Lett. **56**, 2449 (1986); J. P. Pique, Y. Chen, R. W. Field, and J. Kinsey, Phys. Rev. Lett. **58**, 475 (1987).
[39] T. Guhr and H. A. Weidenmüller, Chem. Phys. **146**, 21 (1990); U. Hartmann, H. A. Weidenmüller, and T. Guhr, *ibid*. **150**, 311 (1991).
[40] T. A. Brody, Lett. Nuovo Cimento **7**, 482 (1973).
[41] E. Haller, H. Köppel, and L. S. Cederbaum, Chem. Phys. Lett. **101**, 215 (1983); Phys. Rev. Lett. **19**, 1665 (1984).
[42] R. J. Bell and P. Dean, Faraday Discuss. Chem. Soc. **50**, 55 (1970).
[43] E. J. Heller, J. Chem. Phys. **72**, 1337 (1980); E. J. Heller and M. J. Davis, *ibid*. **86**, 2118 (1982); E. B. Stechel and E. J. Heller, Annu. Rev. Phys. Chem. **35**, 563 (1984).
[44] E. J. Heller and R. L. Sundberg, in *Chaotic Behavior of Quantum Systems*, NATO Adv. Study Ser. B Vol. 120, edited by G. Casati (Plenum, New York, 1985), p. 255.
[45] E. J. Heller, J. Chem. Phys. **92**, 1718 (1990).
[46] M. L. Goldberger and K. M. Watson, *Collision Theory* (Wiley, New York, 1964).
[47] B. Carmeli and A. Nitzan, J. Chem. Phys. **72**, 2054 (1980).
[48] B. Carmeli, R. Tulman, A. Nitzan, and M. H. Kalos, Chem. Phys. **72**, 363 (1982).
[49] S. D. Druger, J. Chem. Phys. **68**, 5250 (1978).
[50] H. Kono, S. H. Lin, and E. W. Schlag, J. Chem. Phys. **77**, 4474 (1982).
[51] M. Aoyagi and S. K. Gray, J. Chem. Phys. **94**, 195 (1991).
[52] A. B. McCoy, D. C. Burleigh, and E. L. Sibert III, J. Chem. Phys. **95**, 7449 (1991).
[53] D. C. Burleigh and E. L. Sibert III, J. Chem. Phys. **98**, 8419 (1993).
[54] H. Kono, Y. Nomura, and Y. Fujimura, Adv. Chem. Phys. **80**, 403 (1991).
[55] M. Terazima, S. Yamauchi, and N. Hirota, J. Chem. Phys. **83**, 3234 (1985); J. Phys. Chem. **89**, 1220 (1985).
[56] H. Hayashi and S. Nagakura, Mol. Phys. **24**, 801 (1972).
[57] R. D. Levine, Adv. Chem. Phys. **70**, 53 (1988).
[58] I. C. Percival, Adv. Chem. Phys. **36**, 1 (1977).
[59] M. V. Berry, J. Phys. A **10**, 2083 (1977); M. V. Berry, J. H. Hannay, and A. M. Ozorio de Almaida, Phys. D **8**, 229 (1983); M. V. Berry, in *Chaotic Behaviour of Deterministic Systems*, edited by G. Iooss, R. Helleman, and R. Stora (North-Holland, New York, 1983), p. 171.
[60] P. O'Connor, J. Gehlen, and E. J. Heller, Phys. Rev. Lett. **58**, 1296 (1987).
[61] P. Pechukas, Phys. Rev. Lett. **51**, 943 (1983).
[62] J. H. Van Vleck, Rev. Mod. Phys. **23**, 213 (1951).
[63] W. T. Raynes, J. Chem. Phys. **41**, 3020 (1964).
[64] W. T. Raynes, J. Chem. Phys. **44**, 2755 (1965).
[65] M. E. Kellman and L. Xiao, J. Chem. Phys. **93**, 5821 (1990); J. P. Pique, J. Manners, G. Sitja, and M. Joyeux, *ibid*. **96**, 6495 (1992); A. D. Bykov, O. V. Naumenko, L. N. Sinitsa, B. P. Winnewisser, M. Winnewisser, P. S. Ormsby, and K. Narakari Rao, J. Mol. Spectrosc. **166**, 169 (1994).
[66] N. Ohta and T. Takemura, J. Phys. Chem. **94**, 3466 (1990); J. Chem. Phys. **93**, 877 (1990).

[67] H. Kono, Chem. Phys. Lett. **214**, 137 (1993).
[68] R. Kosloff, J. Phys. Chem. **92**, 2087 (1988); Annu. Rev. Phys. Chem. **45**, 145 (1994); C. Leforestier *et al*., J. Comput. Phys. **94**, 59 (1991).
[69] M. D. Feit, J. A. Fleck, Jr., and A. Steinger, J. Comput. Phys. **47**, 412 (1982); H. Kono and S. H. Lin, J. Chem. Phys. **84**, 1071 (1986); H. Kono and Y. Fujimura, Chem. Phys. Lett. **184**, 497 (1991); M. Suzuki, Phys. Lett. **146**, 319 (1990); A. D. Bandrauk and H. Shen, Chem. Phys. Lett. **176**, 428 (1991).